Review

SARS-CoV-2 M^{pro} Inhibitors: Achieved Diversity, Developing Resistance and Future Strategies

Conrad Fischer * and **Jenson R. Feys**

Department of Chemistry and Physics, Barry University, 11300 NE 2nd Ave., Miami Shores, FL 33161, USA
* Correspondence: cfischer@barry.edu

Abstract: While the COVID-19 pandemic seems to be on its decline, the unclear impacts of long-COVID cases, breakthrough infections in immunocompromised individuals, vaccine hesitancy, and inhomogeneous health-care accessibility constitute a not to be underestimated threat. These cases, along with pandemic preparedness, ask for an alert identification of new drugs and the optimization of existing drugs as therapeutic treatment options for this and potential future diseases. M^{pro} inhibitors were identified early on as potent drug candidates against coronaviruses, since they target viable processing machinery within the virus, i.e., the main protease that cleaves the polyproteins encoded by the viral RNA into functional proteins. Different strategies, including reversible and irreversible inhibition as well as allosteric inhibitors, mostly from drug repurposing endeavors, have been explored in the design of potent SARS-CoV-2 M^{pro} antivirals. Ambitious screening efforts have uttered an outstanding chemical and structural diversity, which has led to half a dozen lead compounds being currently in clinical trials and the emergency FDA approval of ritonavir-boosted nirmatrelvir as a COVID-19 therapeutic. This comprehensive analysis of the achieved inhibitor diversity sorted into irreversible, reversible, and allosteric M^{pro} binders, along with a discussion of emerging resistance reports and possible evasion strategies, is aimed at stimulating continuing M^{pro} drug design efforts.

Keywords: SARS-CoV-2 M^{pro} inhibitor; SARS-CoV-2 3CL; COVID-19 therapy; allosteric inhibitors; cysteine protease; main protease

1. Introduction

With the current COVID-19 pandemic slowly transitioning to its endemic state, we are confronted with a devastating reality: over 6.6 million deaths worldwide between January 2020 and December 2022, persistent long-COVID cases, and ~3 million confirmed weekly infections (as of December 2022) continue to dramatically impact the socioeconomical motor of society [1]. The vaccination campaign, along with persistent viral exposure, is thought to result in herd immunity; however, the highly adaptive nature of the vaccine targeted spike protein [2,3], campaign fatigue, and globally inhomogeneous vaccine access constitute viral escape routes that fuel a continuous endemic. Mutational analysis of the current SARS-CoV-2 and genomic comparison with previous coronaviruses suggest alternate targets with significantly lower mutation rates and higher structural conservation [4,5]. These include functional proteins that can be targeted with small-molecule inhibitors, which, compared to vaccines, have generally accepted advantages of easier formulation and production, storage, and administration. Among these, two viable main proteases, namely, PL^{pro} and M^{pro}, show a high sequence identity of 86% [6] and 96% [7] between SARS-CoV and SARS-CoV-2, thus reflecting druggable molecular targets. Of the two main proteases, M^{pro} seems the more beneficial target for small-molecule inhibitor development for the following reasons:

- The smaller, spatially more defined active site of M^{pro}, allowing the synthesis of smaller and stiffer inhibitors, whereas efficient binding to PL^{pro} usually relies on tight distal inhibitors [8].

- Dimerization of M^{pro} for activity and close proximity of active site and dimerization interface, suggesting inhibitor design that additionally prevents dimerization [9].
- The lower mutation rates of M^{pro} (nsp5) compared to PL^{pro} (nps3), mitigating the risk of mutation-mediated drug resistance [4].
- Less off-target effects expected, since M^{pro}'s glutamine (Gln) cleavage site recognition is unique and has not been not observed for any human protease. PL^{pro} inhibitors might interfere with human ubiquitin binding motives [10].

Coronavirus replication relies on the expression of two overlapping polyproteins (pp1a and pp1b) as well as four structural proteins encoded by the viral RNA. Both polyproteins liberate vital proteins needed for replication by the action of the main proteases. M^{pro}, a 3-chymotrypsin-like protease (3CL), performs 11 cleavages, whereas PL^{pro} performs only three cleavages, and M^{pro} uniquely recognizes a glutamine in P1 and small, nonpolar residues in P1′ and P2.

This review aims to highlight the current landscape of SARS-CoV-2 M^{pro} inhibitors with emphasis on the mechanistic differences in inhibition and achieved efficacies. Therefore, Pubmed and SciFinder databases were cross-searched using the search term string "SARS-CoV-2 M^{pro} inhibitor" OR "SARS-CoV-2 3CL inhibitor", excluding in silico studies using the NOT "in-silico" term. The ~900 research articles found dating January 2020–November 2022 were sorted manually into three groups: irreversible competitive, reversible competitive, and noncompetitive/allosteric inhibition strategies, and reflect on structure optimization efforts as well as pitfalls. Only chemically synthesized or repurposed drugs that have been biochemically tested and ideally verified by co-crystallization are considered here. Their efficacy, potency, and toxicological data along with available pharmacokinetic profiles are compared. As there is growing evidence for potential viral resistance of some of these inhibitors, including the FDA-approved paxlovid M^{pro} inhibitor nirmatrelvir, we summarize recent reports and point to potential extended therapy solutions.

2. Competitive Inhibitor Design Strategies

M^{pro} is a homodimeric cysteine protease, and effective inhibition of the active site relies on the covalent interaction with the catalytic dyad consisting of cysteine residue 145 (Cys145) located on domain II and histidine 41 (His41) located on domain I (Zhang 2020, [7,11] (Figure 1). Nucleophilic attack of the inhibitor by the cysteine thiolate is preceded by His41-moderated thiol deprotonation, increasing sulfur nucleophilicity [12]. This reflects a generally accepted two-step mechanism that is different from the mechanism of serine proteases such as chymotrypsin that have a catalytic triad that supports a concerted mechanism. Tight binding of the inhibitor causes a slight conformational change that brings both catalytic residues into proximity, thus initiating covalent interaction with the inhibitor warhead. Promiscuity in M^{pro} seems to follow the general trend of being somewhat higher than that in serine proteases [13], as indicated by the longer distance between the dyad residues, giving rise to various peptide and nonpeptide inhibitor geometries and different warhead chemistries. The PDB currently hosts 294 structures of covalently bound competitive M^{pro} inhibitors, which serve as a basis for the structural and mechanistic analysis in this chapter. Chemoinformatic analysis indicates that the vast majority of crystallized inhibitors follow Lipinski design rules, including a molecular weight below 500 Da ($M_{w,aver}$ = 449.5 ± 144.9 g/mol). Aside from covalently bound inhibitors, which are covered in the first part of this chapter, an increasing number of inhibitors that are noncovalently bound in the active site can be found in the recent literature, and these are described in a third subsection. These generally tend to be smaller in size ($M_{w,aver}$ = 346.8 ± 122 g/mol), as is obvious from the comparative structural analysis of their PDB entries (123 PDB structures in total).
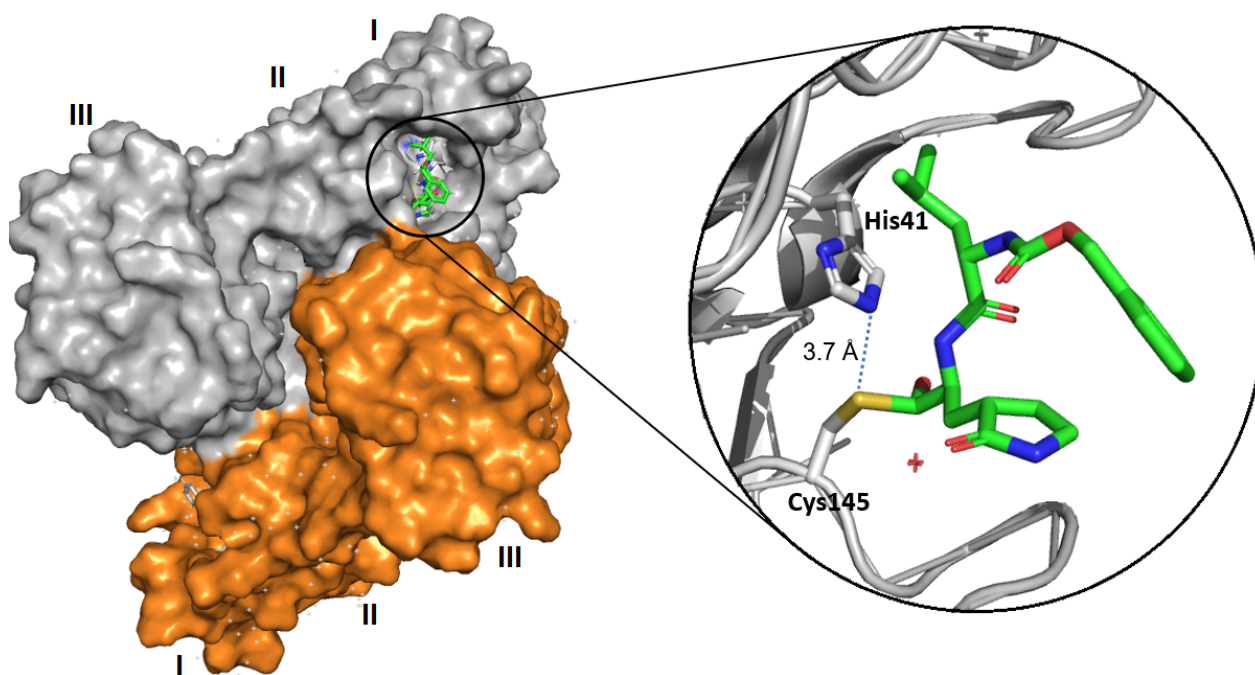
Figure 1. Dimeric structure of SARS-CoV-2 M^{pro} bound to the reversible inhibitor GC376 (PDB 6wtk). The catalytic dyad residues His41 and Cyst145 and a water molecule moderate the chemical attachment of the inhibitor.

2.1. Predominantly Irreversible Warheads

The search for SARS-CoV-2 M^{pro} inhibitors was initiated by a structure-based high-throughput screening of a >10,000 compound database of approved drug molecules, advanced clinical trial drug candidates, and other bioactive compounds. The pseudo-tetrapeptide N3, a Michael acceptor, previously reported as a SARS-CoV and MERS-CoV M^{pro} inhibitor, was found to bind SARS-CoV-2 M^{pro} time-dependently with $k_{obs}/[N3]$ of 11,300 M^{-1}s^{-1} [14] (Figure 2; Table 1). A plaque reduction assay (VeroE6 cells) provided an EC$_{50}$ value of 16.77 µM. The crystal structure of the SARS-CoV-2 M^{pro} complex (PDB 6lu7) confirms the β-vinyl carbon being covalently bound to Cys145's sulfur atom (1.8 Å C-S distance; Figure 2). The P1 lactam ring is held in position by various contacts, including His163, Glu166, and backbone atoms of Phe140, Asn142, and His172 and two water molecules. The side chain of Leu in P2 fits into the hydrophobic enzyme S2 pocket, maintaining several van-der-Waals interactions. The isopropyl group of Val in P3 is solvent-exposed, while Ala in P4 is surrounded by Met165, Leu167, Phe185, Gln192, and Gln189. The same screening study also revealed the 5-hydroxytryptamine receptor antagonist cinanserin as an M^{pro} binder (IC$_{50}$ = 125 µM; EC$_{50}$ (VeroE6) = 20.61 µM), reflecting another example of a repurposed drug that is known as a potent inhibitor of other coronaviruses [15].
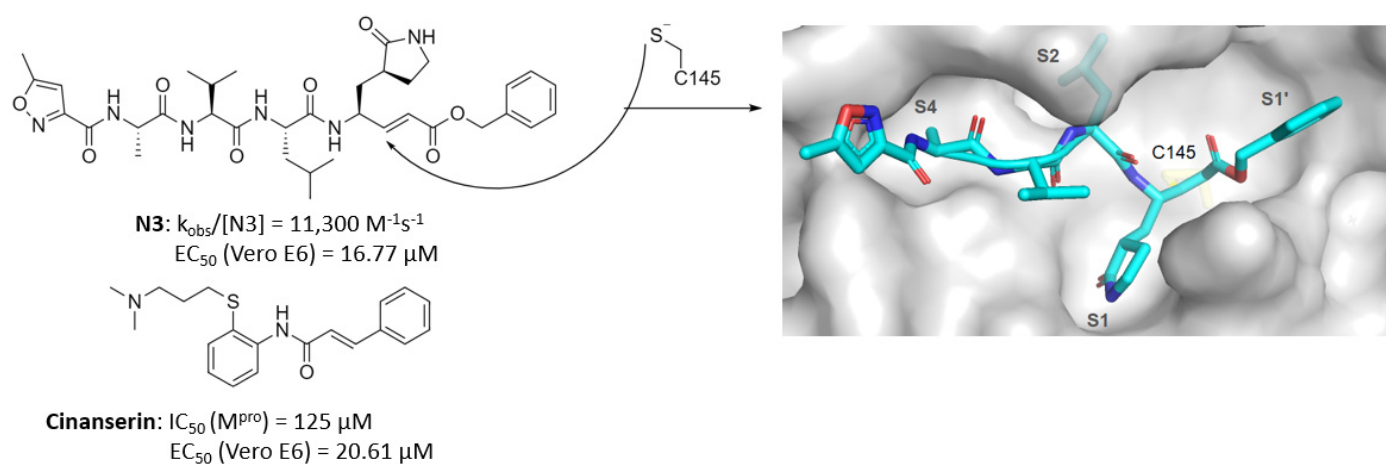
Figure 2. Chemical structure, M^pro binding affinity and antiviral activity of Michael acceptor compounds N3 and cinanserin [14]. The X-ray structure confirms covalent bond formation of N3′s β-vinyl carbon with the Cys145 thiolate (PBD 6lu7).

Cinanserin also resembles an α,β-unsaturated carbonyl drug, which is supposed to covalently bind to Cys145 similarly to N3; however, crystal structure confirmation of this interaction is yet not available. Pharmacological profiles for both drugs have not been accessed; however, toxicological data point to an acceptable safety level (CC$_{50}$ >130 μM (N3) and >200 μM (cinanserin)) [14]. In vitro screening of successful SARS-CoV M^pro inhibitors uncovered the N3 analog **1** as a nanomolar inhibitor of SARS-CoV-2 M^pro (IC$_{50}$= 0.15 μM), able to inhibit replication in VeroE6 cells (EC$_{50}$ = 2.88 μM) [16]. In the crystal structure, inhibitor **1** forms a covalent bond between its β-vinyl carbon and the Cys145 sulfur atom of the main protease (PDB 7jt7 and 7jw8). The ester portion expands into subsite S1′, the γ-lactam ring in P1 is stabilized in S1 by hydrogen bonding involving Phe140, His164, and His166, and the hydrophobic leucine and O-tert-butyl threonine side chains occupy S2 and the surface S3 subsites, respectively. Virtual screening efforts to develop peptidomimetic N3 analogs resulted in a series of α,β-unsaturated carbonyl compounds with variable hydrophobic P1–P3 substituents. Biological evaluation of the promising lead compound **2** from this set found only moderate M^pro inhibition (IC$_{50}$ = 47 μM, [17]). In a search to expand the chemical space of anti-SARS-CoV-2 M^pro α,β-unsaturated carbonyl drugs, recently, also nonpeptidomimetic compounds have been designed [18]. They feature a fused benzo[b]-[1,4]oxazinone-imidazo [2,1-b]thiazole system, which beneficially orients substituents on the aromatic portion of these molecules towards the main protease subsites, as suggested by molecular docking. Biological testing revealed compound SIMR-2418 (Figure 3) as a micromolar SARS-CoV-2 M^pro inhibitor (IC$_{50}$ = 21 μM) with acceptable ADME properties (t$_{0.5}$ > 1 h; mouse LMS).

Another virtual screening study identified nonpeptidomimetic acrylamides as cysteine reactive M^pro inhibitors [19]. The most potent compound from this series is only active in its *S*-configuration (IC$_{50}$ =2.9 μM, K$_i$ = 38 μM; Table 1). A co-crystal structure of LON-WEI-adc59df6-47 (PDB 7nw2) confirms covalent bond formation between the β-vinyl carbon and the active site sulfur atom. From the natural pool of Michael acceptors, the flavonoid myricetin was tried for its anti-SARS-CoV-2 properties (Figure 3) [20]. In vitro screening confirmed sub-micromolar inhibition (IC$_{50}$ = 0.2–0.6 μM), and in the solid-state structure, the covalent linkage to C6 of the pyrogallol unit is obvious (PDB 7b3e). Alternatively, a noncompetitive inhibition mechanism is proposed in the literature [21]. Myricetin's carbonyl-rich structure enables stabilization by hydrogen-bonding, which is moderated through active site water molecules [22]. Covalent bond formation via pyrogallol-C6 can be explained by a preceding oxidation of pyrogallol to o-quinone, enabling attack of the nucleophilic Cys145 thiolate. Myricetin was further shown to block viral infection in vitro (EC$_{50}$ = 8 μM (VeroE6, [22]); 0.9 μM (Calu-3, [21]) and reduce lung inflammation in a mouse model of bleomycin-induced pulmonary inflammation, making it potentially useful for

the symptomatic treatment of COVID-19 [23]. To increase potency, myricetin analogs were designed that included compound **3** with a diphenyl phosphate to the 7-OH of myricetin, resulting in a stronger antiviral effect (Figure 3; EC_{50} = 3.15 μM) [22].

An early drug-repurposing study identified the anticancer drug Carmofur, featuring a carbamoyl warhead, as another type of irreversible M^{pro} inhibitor [24] that also inhibits other SARS-CoV-2 target proteases [25]. Upon acylation of Cys145, releasing 5-fluoro-uracil as side product, the 1-hexylcarbamoyl chain maintains several interactions with Gly143 and hydrophobic residues in S2, as obvious from its co-crystal structure (PDB 7buy). Flexibility and small overall size of the active inhibitor result in an IC_{50} of 1.82 μM and a half-maximal effective concentration (VeroE6) of ~25 μM. Cell toxicity was determined to be around 150 μM (Table 1).

Recently, there has been renewed interest in developing optimized peptide and peptide-mimetic inhibitors based on the initial success of Michael acceptor warheads. The exchange of the α,β-unsaturated carbonyl for hydroxymethyl and alkoxymethyl ketones gave rise to another class of potent M^{pro} inhibitors [26,27]. Reaction of these highly electrophilic ketones with the active site thiolate resulted in a hemithioketal that, unlike Michael-type inhibitors, possesses a coordination-relevant OH group supporting additional stabilizing interactions with the active site residues. Among these, the hydroxymethyl ketone PF-00835231 (Figure 4) has been identified as a nanomolar M^{pro} binder (IC_{50} = 0.007 μM) and effective antiviral (EC_{50} = 35.9μM, Vero6, USA/WA1/2020), the potency of which can be increased almost 80-fold by the application of an efflux inhibitor (EC_{50} = 0.46μM, 2μM CP100356; Table 1). Thermal shift assays as well as an X-ray crystal structure (PDB 6xhm) confirm tight binding to the active site, including a dense array of stabilizing hydrogen bonds in S1' (Figure 4) [28]. The compound is safe in cell assays and displays pharmacokinetic profiles in animals (rat, dog, monkey) that were beneficial for preclinical studies (Table 1). Solubility issues and low oral bioavailability (>2% in rat, dog, monkey) can be overcome by transformation of PF-00835231 into its phosphate prodrug PF-07304814, which is suitable for intravenous injection formulation, releasing about 75% active drug by human alkaline phosphatase cleavage [26]. Extension of the C-terminal alcohol by an alkyl or aryl group results in inhibitors with an α-acyloxymethyl ketone warhead. Unlike the hydroxymethyl ketone PF-00835231, acyloxymethyl ketones possess an electrophilic α-carbon that can be attacked by the active site thiolate, resulting in an irreversible covalent bond, as confirmed by the cocrystal structure of **4** (PDB 7mbi; [27]). By experimental variation, benzoyloxymethyl ketones were identified as the most potent M^{pro} inhibitors, with 2,6-disubstituted aryl rings additionally lowering the *pKa* of the corresponding acid, thus reducing IC_{50} values down to single-digit nanomolar (Figure 5). EC_{50} values of **4** and **5** are 0.3 and 0.16 μM, respectively, with no observed cell toxicity up to the highest tested concentration (200 μM) [27]. With a mouse plasma half-life > 4 h, logD of 4.4, and basolateral-to-apical permeability > 20×10^{-6} cm/s, **4** promises beneficial ADME properties and nondiscriminant thiol reactivity. The six-membered lactam ring seems only to have a marginal effect on the potency of these inhibitors. While highly selective for cysteine proteases over other cellular proteases, these inhibitors act promiscuous towards human cathepsin B and S with IC_{50}'s for **4** of 0.2 μM for CatB and 0.05 μM for CatS.
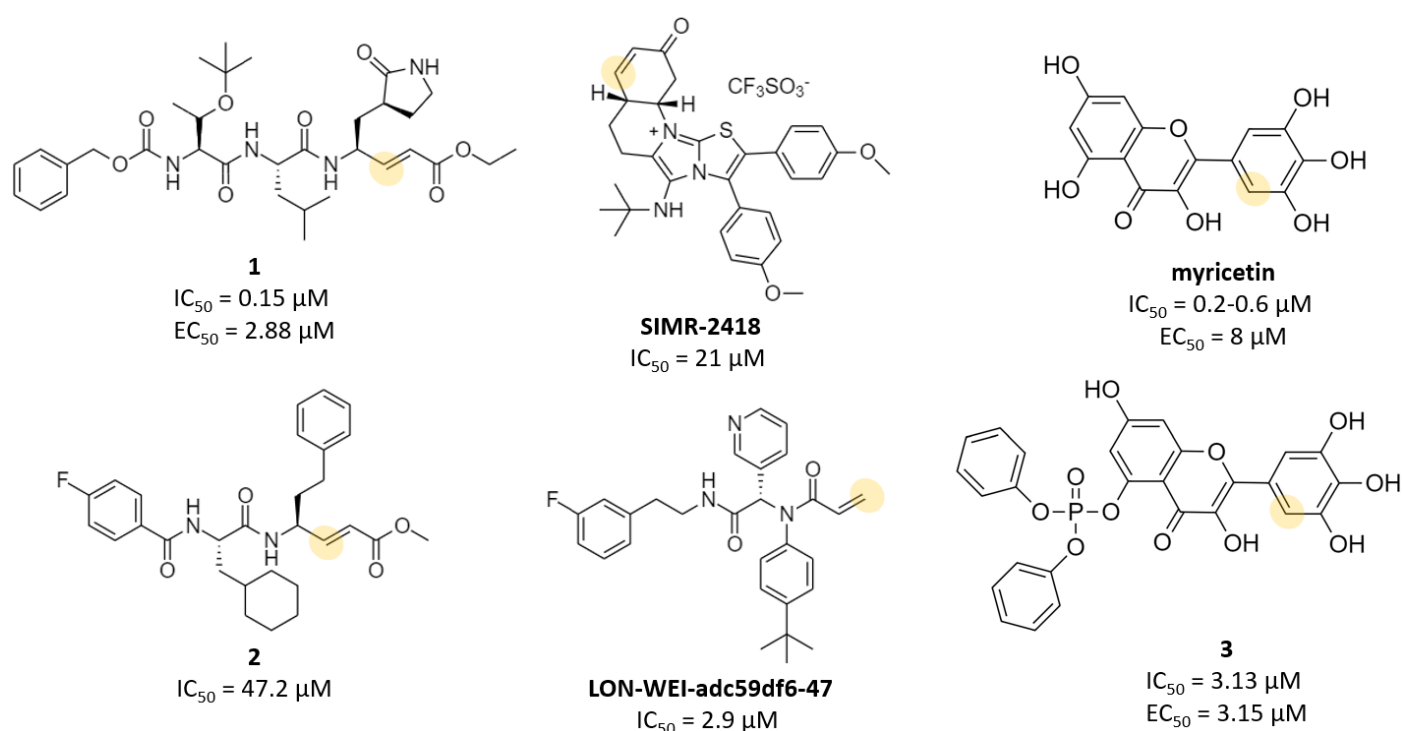
Figure 3. Chemical structure, M$^{\text{pro}}$ binding affinity, and antiviral activity of different designed Michael acceptor inhibitors **1** [16], **2** [17], SIMR-2418 [18], LON-WEI-adc59df6-47 [19], myricetin [22], and **3** [22]. The (β-vinyl)-carbon reacting with Cys145 is highlighted in each structure. In the case of myricetin and its analog **3,** the reactive Michael acceptor structure becomes accessible after oxidation of the pyrogallol unit.

Figure 4. Chemical structure, antiviral, and pharmacokinetic data of PF-00835231 and its drug-precursor phosphate PF-07304814 [26,28].

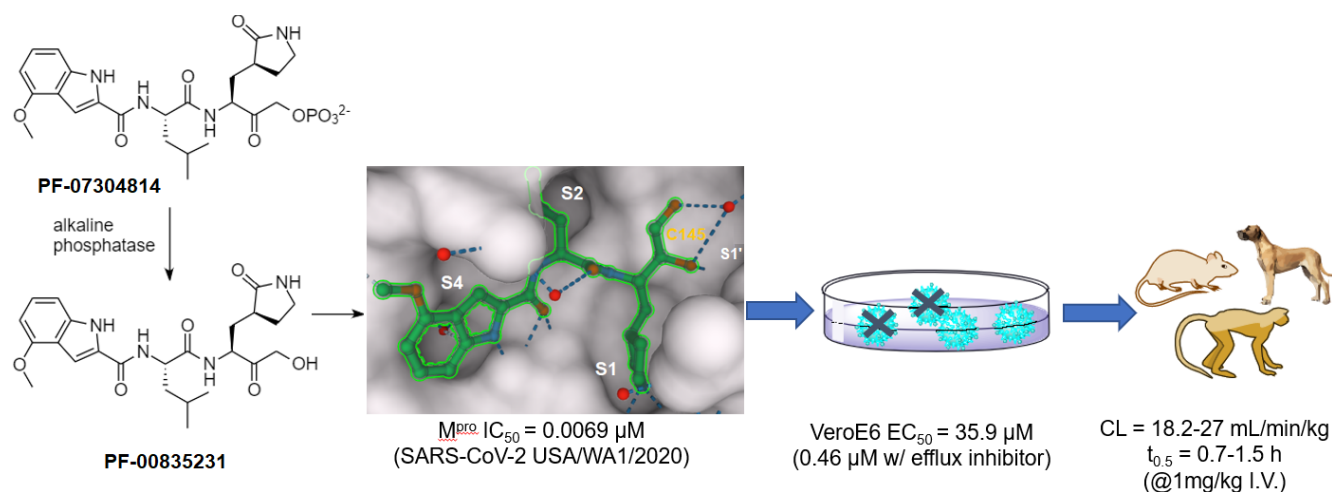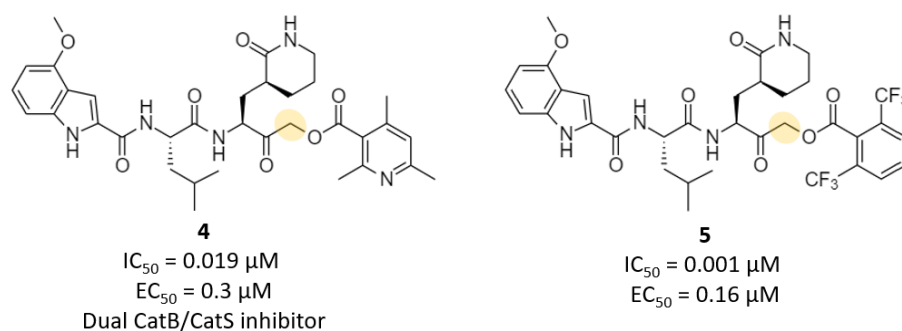**Figure 5.** Chemical structure and inhibition data of α-acyloxymethyl ketones **4** and **5** [27]. The Cys145 reactive α-carbon is highlighted.

Similar to α-acyloxymethyl ketones, α-halomethyl ketones are known as alkylating agents and potent inhibitors for cysteine proteases such as human calpain and cathepsin B [29]. Promiscuity and metabolic stability issues [30] need to be addressed to develop highly selective agents against SARS-CoV-2 M^{pro}. Although peptidic α-halomethyl ketones occur as synthetic intermediates towards α-acyloxymethyl ketones, their inhibitory action towards SARS-CoV-2 M^{pro} has not been tested in the recent literature, probably due to the mentioned lack of selectivity. Structural design therefore seems to concentrate on more specific peptide mimetics such as α-chloroacetamide **6,** which has been identified as a potent SARS-CoV-2 M^{pro} inhibitor (IC_{50} = 0.4 μM) in a comprehensive in vitro study [31].

The crystal structure of **6** confirms displacement of the chloride by the active site thiolate and covalent bond formation (PDB 7mlf). The pyridine sits in the S1 pocket, fixed by a hydrogen bond with the nearby His163, the tert-butylphenyl substituent spreads out into S2, maintaining hydrophobic interactions, and the cycloalkyl group expands towards S4 (Figure 6). Structural optimization of the "side chain" residues shows that a smaller cyclopentyl ring (R3) gives slightly better (IC_{50} = 0.38 μM) and 4-pyridyl or 5-methylpyrazin-2-yl moieties in R1 slightly worse (IC_{50} = 0.8–1 μM) inhibition. Regarding the warhead, a chloromethyl group is more effective than fluoromethyl is, as a consequence of the higher electrophilicity of C-Cl. This electrophilicity can even be further increased by attachment of a second or third halogen, as demonstrated in a related study by Ma et al. using a slightly altered backbone structure [32]. The α,α-dichloroacetamide Jun9-62-2R, accessible by a simple one-pot Ugi four-component reaction, shows beneficial inhibitory data (IC_{50} = 0.43 μM; EC_{50} = 0.9 μM) and low cell cytotoxicity (CC_{50} > 100 μM, Vero6; Table 1). The tribromoacetamide Jun9-88-2R is even more potent (IC_{50} = 0.08 μM; EC_{50} = 0.58 μM) but has a significant lower therapeutic index (CC_{50} = 5.5 μM, Vero6), likely due to interference with other vital proteases that seems predictable for this substitution pattern [33]. Within their comprehensive SAR study, the authors found a tighter inhibition for the *R*-configurated isomers, as observed from the cocrystal structure of Jun9-62-2R (PDB 7rn1, Figure 6). A noteworthy, optimized framework uses an α-chloro-α-fluoroacetamide moiety as warhead, allowing for a strong and selective inhibition of SARS-CoV-2's main protease [34]. A lead derivative from this series, **7**, with a p-pentafluorosulfanyl phenyl group in P2 and a 5-pyrimidinyl group in P1, has an IC_{50} of 0.056 μM (K_i = 1.34 μM) and acts selectively only in its (*R,R*)-*cis* configuration. More recently, novel pyrazoline skeleton derivatives bearing a chloroacetamide warhead also showed promising SARS-CoV-2 M^{pro} inhibition [35]. A lead compound from this series, **8**, has an IC_{50} of 0.53 μM in its *R*-configuration, while the *S*-enantiomer is five times less active. The crystal structure of this compound interestingly shows no occupants in the coordination-rich S1 and S2 subsite; therefore, the 3-phenyl substituent points in the S4 direction and the 5-quinoxalin-6-yl group towards S1 (Figure 6). Instalment of a benzene on C4 and optimization of the C3 substituent gave an even tighter M^{pro} binder, as confirmed by a fluorescent substrate assay. Nonpeptidomimetic chloroacetamide-based inhibitors have been developed in silico; however, likely due to more flexible backbone geometries, none of the tested lead compounds have sub-micromolar inhibition capacity [36]. None of the herein presented

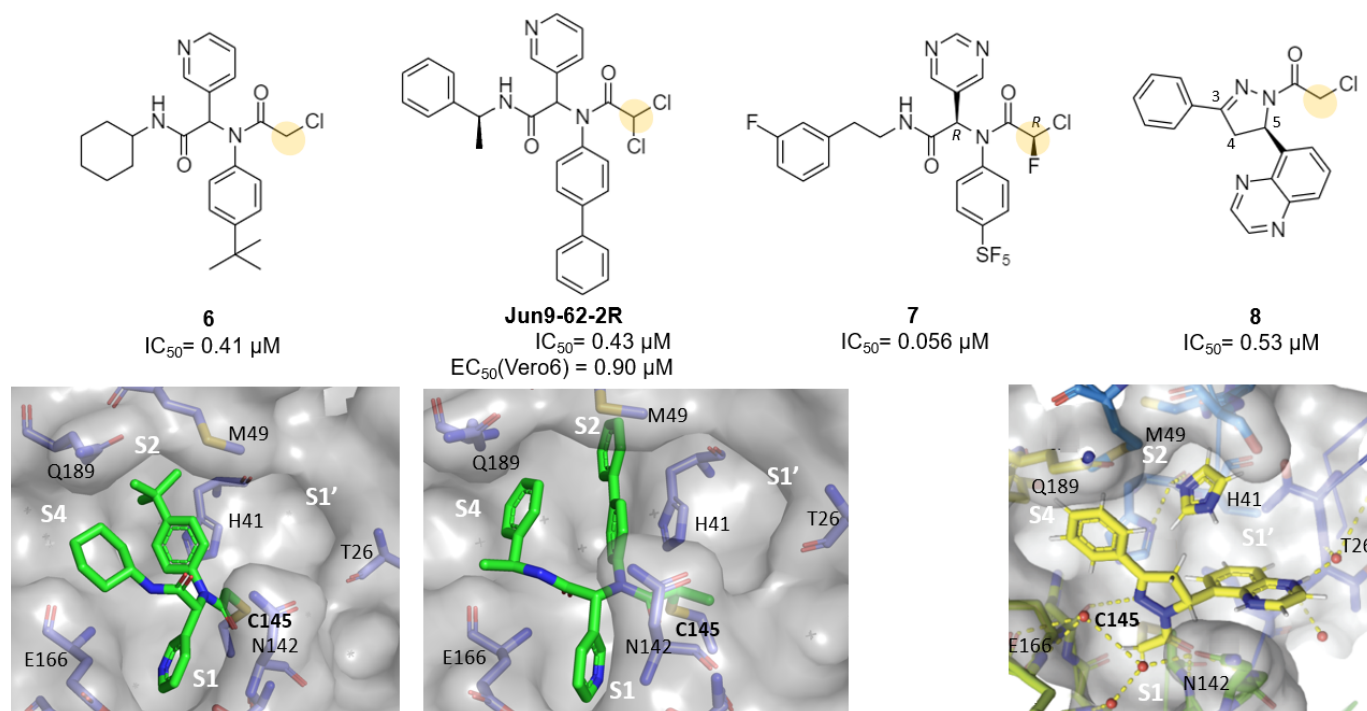inhibitors with chloromethyl ketone warhead have been tested for their pharmacokinetic parameters yet.

Figure 6. α-Chloroacetamides **6** [31], **Jun9-62-2R** [32], **7** [34], and **8** [35] with SARS-CoV-2 antiviral data. X-ray cocrystal structures of **6** (PDB 7mlf), **Jun9-62-2R** (PDB 7rn1), and **8** [35] indicate a covalent bond to the inhibitor's α-carbon atom (highlighted in structures).

Vinyl sulfones are another known warhead for irreversible cysteine protease inhibition [37]. Upon reaction with the active site thiolate, they establish a covalent bond with the inhibitor β-vinyl carbon atom. Decorating the discussed pyrazoline skeleton with such a functionality results in the nanomolar SARS-CoV-2 M^{pro} binder **9** (Figure 7, IC$_{50}$ = 0.035 µM), which shows promiscuity to other coronaviruses, including SARS-CoV, HCoV-NL63, IBV, and HCoV-229E [35]. Other nonpeptidic inhibitors with vinyl sulfone warheads have been developed based on the successful α-chloroacetamide **6**. Swapping out the warhead gives molecule **10** with a IC$_{50}$ of 0.42 µM, which was further optimized by tuning the P3 residue to a 3-chlorophenyleth-2-yl group (**11**; IC$_{50}$ = 0.17 µM) [31]. Isothermal titration calorimetry as well as a crystal structure of **10** (PDB 7mlg) confirm covalent bond formation. The orientation of the molecule in the active site is due to the unchanged P1 and P2 residues almost identical with **6**.
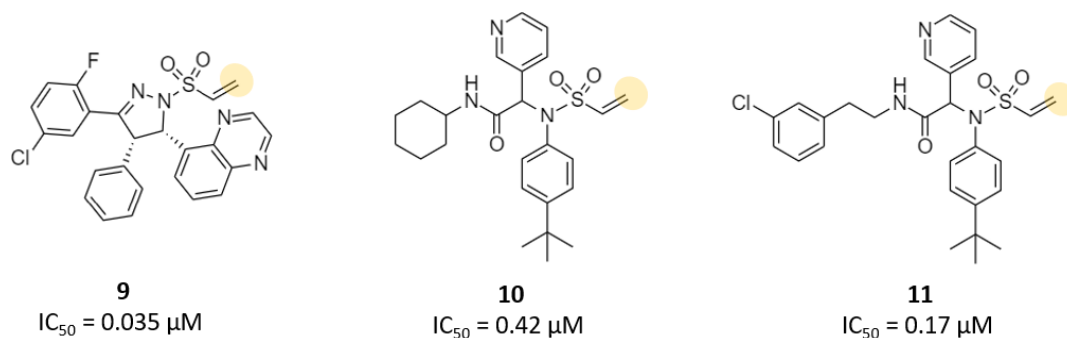

Figure 7. Irreversible M^{pro} inhibitors **9** [35], **10** [31] and **11** [31] with reactive vinyl sulfone group.

Inhibitors with an ester warhead are another category of irreversible M^{pro} agents that has been considered in drug development during this pandemic. Nucleophilic attack of the thiolate results here in the departure of a leaving group and irreversible enzyme acylation. Interestingly, usage of this warhead has so far been limited to small-molecule inhibitors involving rigid pyridine and/or indole systems, exemplified by the molecule GRL-0820 (Figure 8). Among a screen of structural analogs, GRL-0820 stands out with an M^{pro} IC_{50} of 0.073 µM and tolerable anti-SARS-CoV-2 activity (EC_{50} = 15 µM, VeroE6, [38]). Alternate connection or aromatic substitution of the indole unit leads to even more potent M^{pro} binders [15,39]; however, the viral activity of these ester compounds is either unknown [39] or negligible [15]. Recently, a similarly rigid 5-chloropyridinyl ester of salicylic acid was proposed as a drug candidate [40], showing micromolar potency and anti-SARS-CoV-2-viral activity (**12**, IC_{50} = 4.9 µM, EC_{50} = 25 µM). Pharmacokinetic evaluation of ester warhead inhibitors is still pending.

GRL-0820
IC_{50} = 0.073 µM
EC_{50} = 15 µM

12
IC_{50} = 4.9 µM
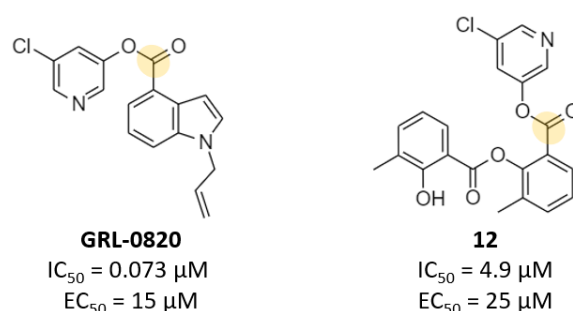EC_{50} = 25 µM

Figure 8. Chemical structure and antiviral data of ester inhibitors **GRL-0820** [38] and **12** [40].

Table 1. Different warhead chemistries, antiviral, and pharmacokinetic data of irreversible SARS-CoV-2 M^{pro} inhibitors.

Warhead	Drug Example [a]	Efficacy	Potency	Toxicology	Pharmacology			Lit.
		K_i/IC_{50} (µM)	EC_{50} (µM)	CC_{50} (µM)	$t_{0.5}$ (h)	C_{max} (ng/mL)	Clear. (mL/min/kg)	
Michael acceptor	N3, Cinanserin, **1**	- 1: 0.15 (IC_{50})	N3: 16.77 1: 2.88	N3: >130 1: >200	-	-	-	[14] [16]
Acrylamide	LON-WEI-adc59df6-47	2.9 (IC_{50}) 38.4 (K_i)	-	-	-	-	-	[19]
Carbamoyl	Carmofur	1.82	24	133	-	-	-	[24]
Hydroxymethyl ketone	PF-00835231	0.0069 (IC_{50})	0.46 [b]	>50 (VeroE6)	0.72 (rat)	1250 (rat)	27 (rat)	[26]
Acyloxymethyl ketone	4, 5	0.001	0.16	>200	>4 (mouse-plasma)	-	-	[27]
Chloroacetamides	**6, Jun9-62-2R, Jun9-88-2R**	6a: 0.4 (IC_{50}) Jun9-62-2R: 0.43 (IC_{50}) Jun9-88-2R: 0.08 (IC_{50})	6a: -Jun9-62-2R: 0.9 Jun9-88-2R: 0.58	6a: -Jun9-62-2R: >100 Jun9-88-2R: 5.48	-	-	-	[31]
Chlorofluoro-acetamides	**7**	0.056 (IC_{50}) 1.34	-	-	-	-	-	[34]
Vinylsulfonamide	**11**	2.3 (K_i) 0.17 (IC_{50})	-	-	-	-	-	[31]

[a] Bold entries resemble inhibitors corresponding to reported activity, safety, and pharmacology data; [b] using an efflux inhibitor.

2.2. Reversible Warheads

Reversible inhibitors possess a reactive carbonyl function that, upon reaction with the nucleophilic cysteine thiolate, forms a temporary addition product. The resulting covalent bond is less strong than that for the previously described irreversible warheads, thus supporting time-dependent reversal of the binding event and drug clearance. Functional groups that establish a reversible covalent bond include foremost aldehydes, α-ketoamides, and some α-substituted ketones as well as nitriles. Aldehydes and ketones form hemithioacetals, whereas nitriles form a reversible thioimidate (Figure 9). It seems an acceptable consensus that reversible inhibition is preferable as, in general, it allows for

more selective target binding and fewer off-target effects, and promotes bioavailability and efficacy of respective inhibitors and their ultimate clearance from the infected host. It therefore does not surprise that among the 500+ covalent anti-SARS-CoV-2 M[pro] drug candidates, predominantly those with reversible warhead chemistries were forwarded to clinical testing (see next chapter).
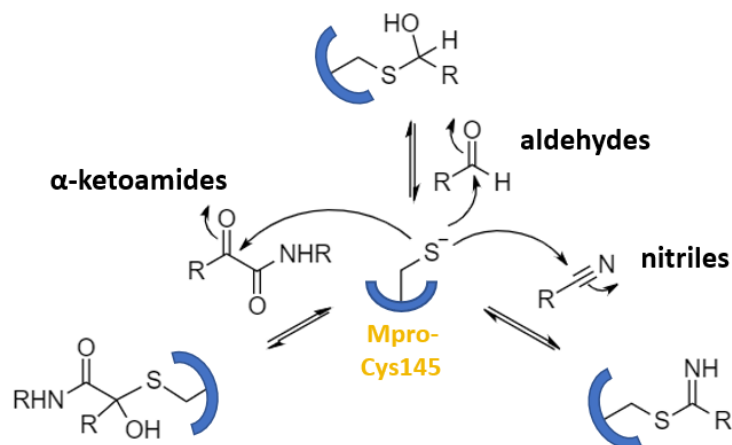

Figure 9. Different reversible M[pro] inhibition mechanisms involving α-ketoamides, aldehydes, and nitriles.

Aldehydes represent the biggest investigational group among reversible SARS-CoV-2 M[pro] inhibitors. Chronologically, the two peptides **13** and **14** were the first tested aldehydes, rationally modeled after successful SARS-CoV M[pro] inhibitors [41]. They feature a γ-lactam group in P1, a six-membered aliphatic or aromatic side chain in P2, and an indole moiety in P3. Both drug compounds show remarkable in vitro activity (IC_{50} = 0.053 and 0.04 μM, **13** and **14**), strong antiviral effect (EC_{50} = 0.53 and 0.72 μM, **13** and **14**), low cytotoxicity, and preferable pharmacokinetic parameters. Beneficial complementarity of the used side chains is highlighted in the obtained X-ray structures (PDB 6lze (**13**) and 6m0k (**14**)): an additional H-bond between the thioacetal –OH group and Cys145 backbone enhances stabilization of the covalent bond. The γ-lactam group maintains H-bonds with Glu166 and His163 and an additional contact with Phe140 in S1, the cycloaliphatic (**13**) or aromatic (**14**) P2 residue penetrates the S2 pocket, supported by several hydrophobic interactions, and the indole moiety is located at the solvent interface (S4).

A structural analog of **14** with a benzyl group in P2 (**15**) shows improved binding (IC_{50} = 0.034 μM) and even better antiviral activity (EC_{50} = 0.29 μM) [42]. Vuong et al. explored the known peptide aldehyde GC373 and its bisulfite adduct GC376 as potent reversible anti-SARS-CoV-2 M[pro] agents [43]. Both drugs were initially investigated as inhibitors of a feline coronavirus (FCoV) that causes a fatal inflammatory disease in cats (feline infectious peritonitis). Under physiological conditions, the bisulfite adduct GC376 reverses to the active aldehyde drug GC373 (Figure 10). Since FCoV and SARS-CoV-2 M[pro] are highly homologous cysteine proteases and share close resemblance of their active site geometries, a repurposing attempt seemed reasonable. Indeed, both drugs proved effective as new anti-COVID-19 agents with half-maximal inhibitory concentrations, M[pro]-IC_{50}, of 0.40 μM (GC373) and 0.19 μM (GC376) [43]. Several hydrogen bonds with the oxyanion hole residues Gly143, Ser144, and Cys145 stabilize the hemithioacetal of GC373, as is obvious from its cocrystal structure [43,44]. Inhibitor interactions in S1 and S2 are identical to those of the aldehydes **13** and **14**, the benzyloxycarbonyl group in P3 coordinates with Glu166. In the cell infectivity assay, both drugs showed micromolar effectivity (GC373: EC_{50} = 1.5 μM; GC376: EC_{50} = 0.9 μM) and low cell toxicology (CC_{50} for both >100 μM). Efficacy of GC376 against SARS-CoV-2 infection was shown in a transgenic mouse model expressing the human angiotensin-converting enzyme type 2 (K18 hACE2) [45]. Pharmacokinetic profiling performed by Shi et al. indicated a quick and durable uptake of GC376

after intramuscular injection in mice and rats ($t_{0.5}$ = 1.1 h (mice) and 3.9 h (rat)), a high peak plasma concentration, and good clearance [46] (Table 2). Reversibility of GC376 binding was demonstrated with a ^{13}CHO-labeled GC376 derivative in a time-dependent NMR experiment [47]. To find even more potent structural analogs of GC376, the Vederas group explored various synthetic derivatives with different P2 and P3 substitutions for their anti-SARS-CoV-2 behavior [48]. The two lead compounds **16** and **17,** with a cyclopropyl group in P2 and an *m*-halophenyl substituent in P3, were identified in this series, displaying improved IC_{50} values of 0.07 and 0.08 µM, respectively. Both compounds showed slightly better antiviral susceptibility compared to GC376 (EC_{50} = 0.57 and 0.7 µM, respectively) and no cytotoxicity [48]. A crystal structure of **16** with SARS-CoV-2 M^{pro} highlights an enhanced interaction of the P2/P3 groups with respective enzyme subsites (PDB 7lco). Further structural optimization of the GC376 core led to the two potent antiviral drug candidates UAWJ247 (IC_{50} = 0.045 µM) [49] and NK01-63 (coronastat, IC_{50} = 0.016 µM) [50]. The latter compound has a pronounced antiviral effect (EC_{50} = 0.006 µM; Huh-7ACE2-infected cells) and high selectivity over other human proteases. Aside from the common interaction patterns, the NK01-63 cocrystal structure features two additional H-bonds of the P3 trifluoromethylphenyl group to nearby Asn142, reiterating the prominent stabilization effect of halogens (PDB 7tiz). In vitro mice tests confirmed good microsomal stability, and in vivo pharamacokinetic analysis underlined high uptake via both intraperitoneal and oral routes, with an extended half-life in critical tissues such as lung (I.P., $t_{0.5}$ = 2.2 h; P.O. $t_{0.5}$ = 3.4 h). Another example of activity-guided optimization of GC376's structure led to analog **18**, which has a constrained bicyclic ring system in P3 [51]. M^{pro} FRET substrate assay of **18** indicated an IC_{50} of 0.18 µM and nanomolar efficacy in the plaque reduction assay (EC_{50} = 0.035 µM; VeroE6).

Inspired by the structurally related FDA-approved antivirals boceprevir and telaprevir, Xia et al. also synthesized and tested boceprevir/telaprevir-GC376 chimera [52]. Some of these analogs turned out to be nanomolar SARS-CoV-2 M^{pro} inhibitors (**19**: IC_{50} = 0.054 µM; **20**: IC_{50}= 0.051 µM) and (sub)micromolar antivirals (VeroE6, **19**: EC_{50} = 0.37 µM; **20**: EC_{50} = 2.6 µM). X-ray data for both compounds (PDB 7lyi (**19**) and 7lyh (**20**)) confirmed successful insertion of the bicyclic proline moieties into the S2 subpocket. Additional modification of the P3 substituent, as tried in an extensive SAR study by Qiao et al., led to the superior compound MI-23 with an IC_{50} of 0.008 µM [53]. In the cocrystal structure, the extended 1-ethyl-3,5-difluorobenzene substituent in P3 interacts via hydrophobic contacts with nearby Leu167 and Pro168, additionally contributing to a tight fit of this inhibitor. Presumably due to a limited cell membrane permeability, MI-23 and other inhibitors of this series had reduced activity in the cell protection assay (EC_{50} = 5.6 µM), incentivizing the authors to select further structurally modified P3 analogs for pharmacological testing. The analog MI-30 (**21**) with a (2,4-dichlorophenoxy)acetyl group in P3 had a persistent low IC_{50} of 0.017 µM, good in vitro efficacy (EC_{50} = 0.54 µM), no common cell toxicology, and protected transgenic mice that expressed hACE2 against SARS-CoV-2 infection. In an SD rat model, MI-30 showed good in vivo stability ($t_{0.5}$ = 2.35 h), high plasma concentrations (C_{max} = 23582 ng/mL), and sufficient clearance (CL = 17.1 mL/min/kg).

To improve the surface interaction of inhibitory peptides, Yang et al. shifted their focus to optimizing tripeptides as SARS-CoV-2 M^{pro} inhibitors [54]. A potent aldehyde from their series (MPI8) has the common γ-lactam ring in P1, a cyclohexyl group in P2, and a benzyloxycarbonyl-protected tert-butylserine in P3, and displayed an IC_{50} of 0.11 µM and good in vitro antiviral efficacy (EC_{50} = 2.5 µM). Indeed, the cocrystal structure of MPI8 (PDB 7jq5) reveals a bifurcated orientation of the P3 residue covering an extended area of the solvent-exposed S3/S4 site, highlighting enhanced interaction with several hydrophobic M^{pro} residues. In an extended study by the same group, the authors classify MPI8 as dual inhibitor of M^{pro} and cathepsin L, showing nanomolar half-inhibition concentrations for both cysteine proteases [55]. Cathepsin L, among other membrane proteases, is suspected to facilitate coronaviral entry, giving dual inhibitor aldehydes such as MPI8 superior viral-neutralization qualities. This concept was further explored in various drug-repurposing

studies focusing on well-known proteasome inhibitors. As such, MG-132 was shown to effectively bind to and inhibit both SARS-CoV-2 and cathepsin L [56,57]. Another set of studies proved calpain inhibitors II and XII as potent SARS-CoV-2 M^{pro} binders (IC_{50} = 0.97 and 0.45 µM, respectively) with a micromolar antiviral effect [39,58,59].

A second important reversible warhead functional group that has been extensively implemented in M^{pro} inhibitor design comprises α-ketoamides. This function is especially valuable since, in addition to the hemithioacetal generated by the reaction of the ketone with the cysteine sulfur, the neighboring ketoamide can also engage in stabilizing hydrogen bonds. A recurring bonding motif for this function involves a hydrogen bond from the hemithioacetal –OH with His41 and hydrogen bonds from the amide group with backbone amides Gly143, Ser144, and Cys145. Some of the first proposed peptide-based inhibitors during the pandemic were compounds **22** and **23** (Figure 11), prominent SARS-CoV inhibitors. Their sub-micromolar performance against SARS-CoV-2 was confirmed by FRET M^{pro} assay, and optimized compound **23** blocked SARS-CoV-2 viral replication with EC_{50}'s > 5 µM [7,60]. The solid-state structure of **23** with M^{pro} confirms the expected hydrogen bond network around the active site Cys145, orienting the C-terminal benzyl group towards the S1′ site. S1 is accommodated by the five-membered ring glutamine surrogate, S2 hosts the cyclopropyl side chain, and the pyridyl moiety in P3 seems beneficial in supporting additional hydrogen bonds with Glu166 that line up the N-terminal Boc group towards the surface S3 pocket. Beneficial ADME and pharmacokinetic data of **23** (Table 2) suggest pyridone-containing inhibitors as a viable framework towards anticoronaviral drugs. Based on the GC376 core structure, α-ketoamides UAWJ246 and UAWJ248 were developed (Figure 11) [49]. In vitro testing indicated a negligible effect of exchanging the aldehyde for a ketoamide warhead, with UAWJ246 scoring an IC_{50} of 0.045 µM and an EC_{50} of 4.61 µM. Other repurposing studies identified the hepatitis C antivirals boceprevir and telaprevir as promising model compounds to combat SARS-CoV-2 (Figure 11) [61,62]. Cocrystal structures with both drugs confirm hemithioactal formation and a surprisingly snug fit of both drugs into the protease subsites (boceprevir: PDB 6zru; telaprevir: PDB 6zrt). While the IC_{50} of telaprevir was determined as 18 µM [63] and cell studies indicated cytotoxicity above 60 µM [64], boceprevir seemd more active (IC_{50} = 4.13 µM), inhibited SARS-CoV-2 replication with an EC_{50} value of 1.95 µM, and was not toxic in Caco-2 cells (CC_{50} > 100 µM) [61]. A different study found the proteasome inhibitor A, which inhibits proliferation of various cell cancer lines in nanomolar concentrations, a suitable COVID-19 antiviral [65]. The VeroE6 cell assay determined an even better antiviral effect (EC_{50} = 1.28 µM) of A compared to the related tripeptides with an aldehyde warhead.
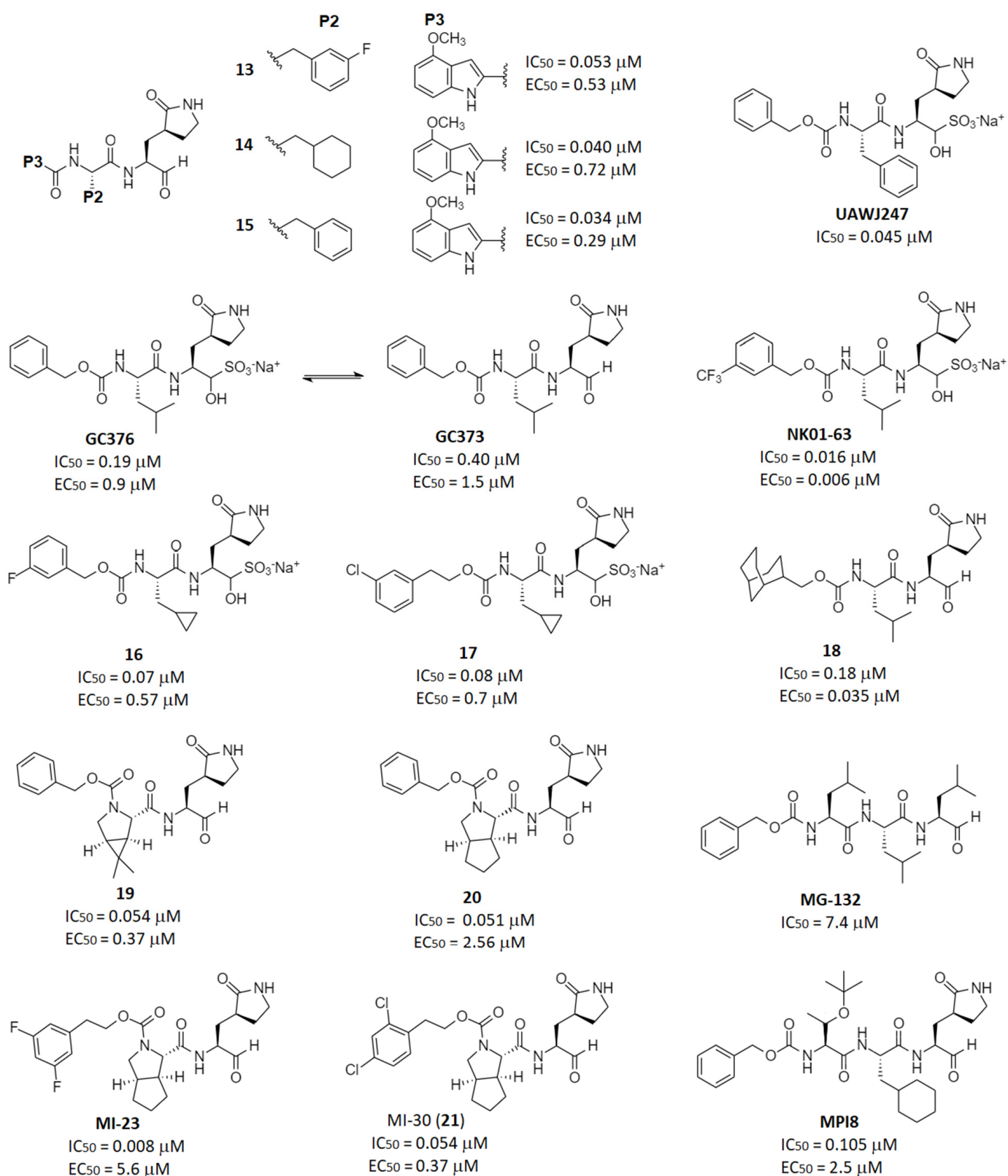
Figure 10. Chemical structures of aldehyde-based M$^{\text{pro}}$ inhibitors **13–15** [41,42], GC376 and GC373 [43], **16** and **17** [48], UAWJ247 [49], NK01-63 [50], **18** [51], **19** and **20** [52], MI-23 and MI-30 (**21**) [53], MPI8 [54], as well as MG-132 [56]. Inhibitory (IC$_{50}$) and antiviral data (EC$_{50}$) are given below each structure.
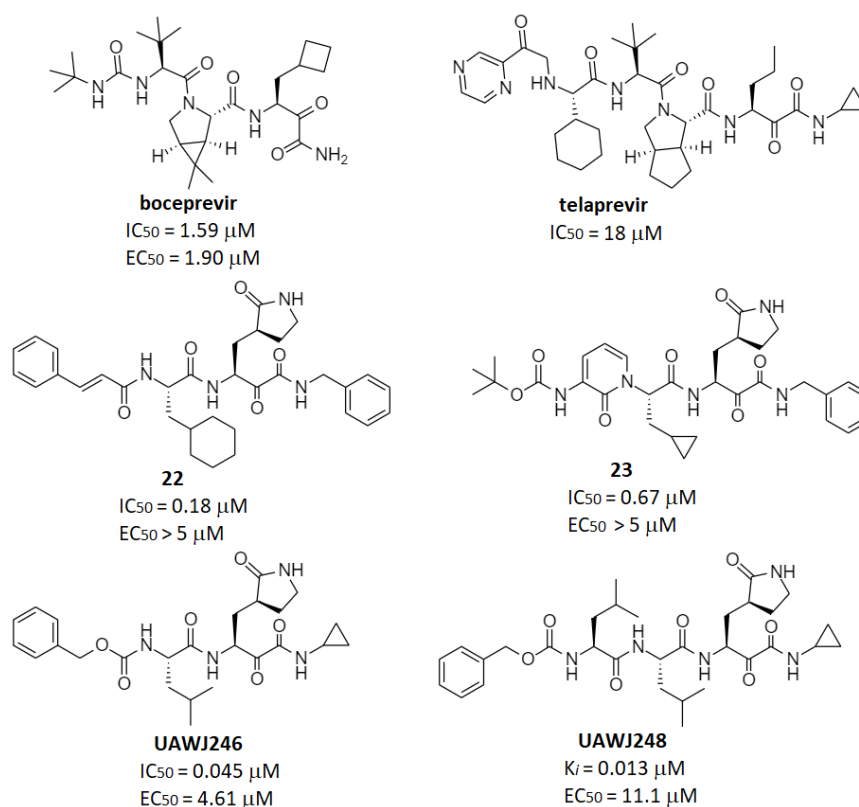
Figure 11. Reversible M^{pro} inhibitors with ketoamide warhead, **22** and **23** [7,60], as well as UAWJ246 and UAWJ248 [49] are based on the FDA-approved hepatitic C (HCV) antivirals boceprevir [61] and telaprevir [62].

A third category of reversible M^{pro} inhibitors uses a nitrile warhead to establish a temporary covalent bond with the enzyme. A nucleophilic Cys145 thiolate attack of the electrophilic nitrile carbon results here in the formation of a reversible thioimidate. Although nitrile-based peptidomimetic SARS-CoV-2 inhibitors developed as past (corona)viral defense agents showed only moderate inhibition success [66], the nitrile function is a chemically valuable way to reduce the number of hydrogen bond donors in the molecule [67]. This feature is helpful for the development of orally available drug candidates, as a reduced number of hydrogen bond donor functions increases drug permeability in the gut. Using this chemical masking strategy, Pfizer chemists developed, in a comprehensive drug development program, nirmatrelvir, influenced by structural optimization of the α-hydroxymethyl ketone PF-00835231 and the benzothiazol-2-yl ketone candidate **24** (Figure 12) [67]. The concept proved successful, with nirmatrelvir showing nanomolar SARS-CoV-2 M^{pro} inhibition ($IC_{50} = 0.019$ μM), a strong antiviral effect ($EC_{50} = 0.075$ μM), and no cell toxicity [68]. The X-ray structure shows thioimidate formation of the inhibitor with Cys145 of the main protease, supported by stabilizing hydrogen bonds of the imine with nearby Gly143 (PDB 7vh8 and 7vlq) [69]. The choice of an N-terminal trifluoroacetyl group in the drug design is supported by stabilizing contacts with Gln192 in the S4 pocket. In vivo animal tests confirmed desired intestinal permeability features, excellent oral bioavailability, and proper drug clearance (Table 2). A mouse-adapted SARS-CoV-2 (SARS-CoV-2 MA10) model responded with significantly reduced virus levels in the lungs after 4 days of a twice-daily treatment regime with nirmatrelvir (300 mg/kg) compared to the placebo group. Excellent in vitro and pharmacokinetic performance as well as favorable off-target selectivity qualified the drug candidate for clinical trials, consequentially leading to emergency FDA approval of nirmatrevir in December 2021. During the preclinical trials, it was found that coadministration of the anti-HIV drug ritonavir increased drug performance due to ritonavir's inhibitory action on CYP-mediated metabolism. This ultimately resulted in

coformulation of nirmatrelvir with ritonavir in the final drug paxlovid. In light of the mutational adaptivity and widespread transmission of different SARS-CoV-2 variants of concern, it can be seen encouraging that several studies confirmed nirmatrelvir's ability to efficiently neutralize infection of beta, delta, and omicron variants of the virus in animal models [70–74]. Regarding effectivity in humans, a manufacturer-conducted study indicated persistent pharmacokinetic performance, viral clearance, and drug safety in healthy participants [75]. Related studies with renally impaired subjects showed increased peak plasma concentrations of the drug and delayed clearance correlating with severity of renal disease, thus recommending a dose reduction for this impairment group [76]. Driven by the success of nirmatrelvir, several analogs with adaptations of the P2 and P3 sites have been developed. A related patent by Pfizer identified compound **25** as a strong main protease binder (K_i = 0.004 μM) and effective SARS-CoV-2 antiviral (EC_{50} = 0.019 μM) [77]. A different group considered elements of GC376 and its derivatives for their inhibitor optimization screening. Among their synthesized compounds, nitrile **26** was the most active in the inhibition assay (IC_{50} = 0.009 μM) and potent in reducing viral replication (EC_{50} = 2.2 μM) [78].

Nirmatrelvir
IC_{50} = 0.019 μM
EC_{50} = 0.075 μM

24

25
K_i = 0.004 μM
EC_{50} = 0.019 μM

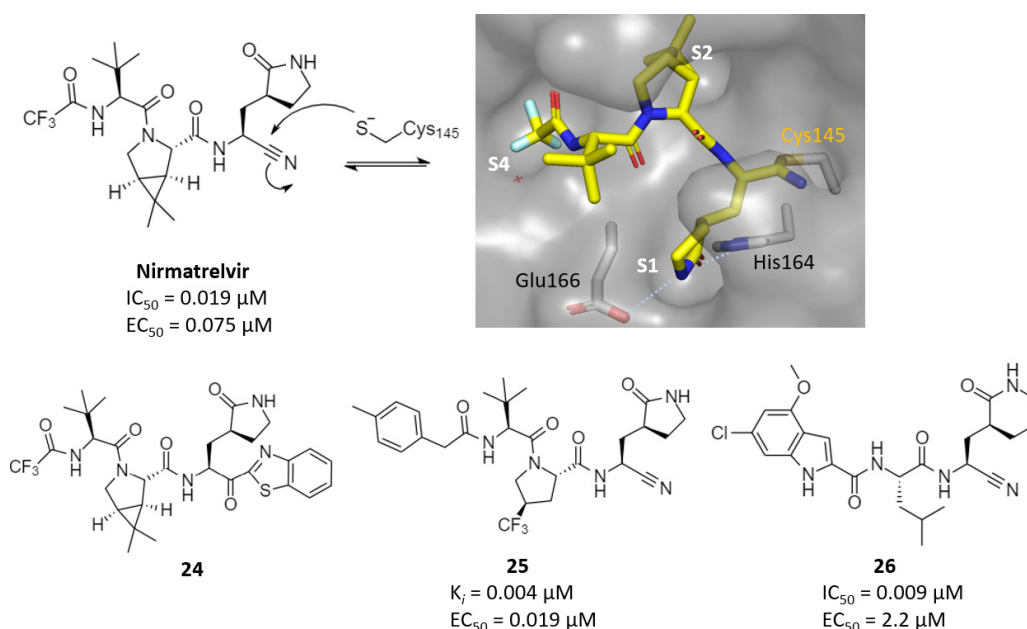**26**
IC_{50} = 0.009 μM
EC_{50} = 2.2 μM

Figure 12. Structure of nirmatrelvir [68], its precursor **24** [67], and analogs **25** [77] and **26** [78]. The crystal structure (PDB 7vh8, 7vlq) highlights covalent attachment (thioimidate formation).

An odd case of covalent inhibition of SARS-CoV-2 M[pro] concerns the repurposing studies of the anti-inflammatory agent ebselen, which has been in the inhibitor race since early 2020. Enzymatic testing indicated strong inhibition and antiviral activity of ebselen (IC_{50} = 0.67 μM, EC_{50} = 4.67 μM, VeroE6) [14,79]. Two inhibition mechanisms are discussed in the literature: covalent attachment to and ultimate selenylation of Cys145 [79] and allosteric inhibition at a dimerization site (discussed later). Covalent inhibition proceeds through S_N-type opening of the benzisoselenazol ring and subsequent hydrolysis, releasing a phenolic byproduct and the selenylated cysteine sulfur, as suggested by DFT and mass spectrometric analysis (Figure 13) [80,81]. The final sulfur selenium adduct was confirmed by X-ray crystallography (PDB 7bak) [79]. Considering the possibility for plural inhibition within M[pro], ebselen analogs were designed and tested. One design avenue considered ebselen derivatives with a modified nitrogen substituent [79], where again it was found that halide substitution beneficially influences inhibitor properties. The most active compound from this series, **27**, showed similar potency to that of the parent ebselen and had about three times improved antiviral activity (EC_{50} = 1.78 μM; VeroE6). Substitution of the

selenium atom for sulfur gives the isosteric compound ebsulfur, which also acts as a potent M^{pro} inhibitor. Among a series of analogs, compound **28** bound with an IC$_{50}$ of 0.11 μM to the target; however, antiviral and pharmacokinetic data have not been reported yet.
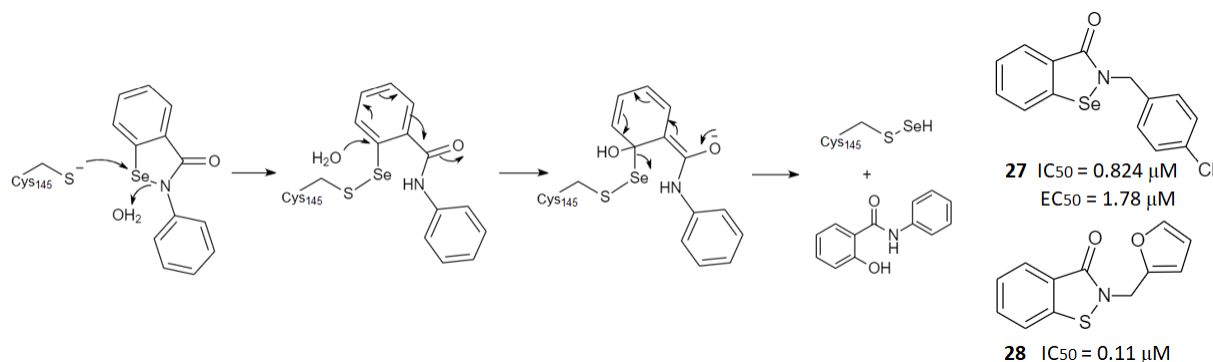

Figure 13. Proposed M^{pro} inhibition mechanism of ebselen and structure of ebselen analogs **27** and **28** [79].

Table 2. Reversible inhibitors of SARS-CoV-2 M^{pro} with inhibitory and pharmacological data.

Warhead	Drug Example	Efficacy	Potency	Toxicology	Pharmacology			Lit.
		IC$_{50}$ (μM)	EC$_{50}$ (μM)	CC$_{50}$ (μM)	t$_{0.5}$ (h)	C$_{max}$ (ng/mL)	Clear. (mL/min/kg)	
Aldehydes	**13–21**, GC376, MPI8, MI-23	GC376: 0.19	GC376: 0.92	GC376: >100 (Vero6)	GC376: 1.1 (mouse), 3.9 (rat)	GC376: 46700 (mouse), 12560 (rat)	GC376: 33.1 (mouse), 20.1 (rat)	[43] [46]
Ketoamides	**23**, UAWJ246	23: 0.67 UAWJ246: 0.045	23: 4–5 UAWJ246: 4.61	UAWJ246: >250 (Vero6)	23: 1.0 (mouse)	23: 334 (mouse)	23: 566 (mouse)	[7] [49]
Nitriles	nirmatrelvir	0.019	0.075	>100 (Vero6)	1.5 (rat, P.O.)	1290 (mouse, P.O.)	-	[68]

2.3. Noncovalent Active Site Inhibitors

A virtual screening study performed by Yang et al. identified Z1759961256 (Figure 14) as one of six hits with micromolar M^{pro} potency and viral activity against SARS-CoV-2 [82]. Similarly, in the optimization of the molecular library probe ML300 in a comprehensive study design, CCF981 evolved as lead compound with a strong M^{pro} inhibition capability (IC$_{50}$ = 0.068 μM) and a pronounced antiviral effect (EC$_{50}$ = 0.56 μM; VeroE6) [83]. The drug binds well into M^{pro}'s active site cavity with the imidazole system pointing towards S1′, the benzotriazole unit in S1, and the m-chlorobenzene occupying S2, as abstracted from the binding modes of structurally similar analog crystal structures. Following the dual inhibitor approach to maximize the antiviral effect, Elseginy et al. synthesized inhibitor **29** (Figure 14) after mapping a >50,000 compound library for structural hits [84]. In vitro tests identified **29** not only as a potent M^{pro} binder (IC$_{50}$ = 0.11 μM) but similarly as a good inhibitor of PL^{pro} and human furin protease. Cell assays indicated cytotoxicity in mammalian cells that were overcome by synthesis of analogs of **29**. Inspired by the weak anti-SARS-CoV-2 M^{pro} activity of the antiepileptic perampanel, Zhang et al. synthesized and tested 27 structural analogs in their search for better inhibitory activity [85]. While most synthesized compounds showed sub-micromolar M^{pro} inhibition, VeroE6 cell assays indicated considerate toxicity. One compound (**30**), however, stood out, having a low M^{pro} IC$_{50}$ of 0.17 μM, potent antiviral effect (EC$_{50}$ = 0.98 μM), and displaying no cell toxicity within the tested concentration range (CC$_{50}$ > 100 μM). The crystal structure of a related analog shows the cloverleaf-like molecular structure occupying three subpockets of the protease (PDB 7l11). Using an in-house structural library, Unoh et al. recently discovered another cloverleaf-like structure that shows beneficial anti-SARS-CoV-2 properties and binds noncovalently in the active site of M^{pro} [86]. Virtual screening with predefined filters that include two hydrogen bond acceptors in S1 and a hydrophobic element in S2

narrowed down the selection of hit structures suitable for biological screening. Among them, the compound S-217622 displayed very strong binding to M^{pro} (IC$_{50}$ = 0.013 μM) and pronounced antiviral effect in the plaque reduction assay (EC$_{50}$= 0.37 μM). Further biochemical assays confirmed that S217622's antiviral activity extends to common SARS-CoV-2 variants, including the omicron strain (EC$_{50}$= 0.29–0.5 μM), while other proteases, including cathepsins and thrombin, remain uninhibited. In the X-ray structure, the 1,3,5-triazine-2,4(1H,3H)-dione core sits in the middle of the catalytical site, with the three wing-like substituents reaching in S1', S1, and S2 pockets (PDB 7vu6). A tight fit is achieved by a dense H-bond network involving Gly146, Ser147, His165, and Glu168 of the enzyme as well as π–π interactions between His43 and the aromatic P2 inhibitor moiety (Figure 14). The superior in vitro performance of S-217622 stimulated in vivo testing in mice infected with SARS-CoV-2 Gamma strain, where viral titers in lung homogenates were determined 12 h after oral dose of S-217622 and 24 h after infection. The drug demonstrated a peak plasma concentration that at all tested doses (2–32 mg/kg single dose, P.O.) was above the protein-adjusted EC$_{50}$, thereby reducing the viral titer at the highest two doses to the detection limit (1.8 log$_{10}$[TCID$_{50}$]/mL). Full pharmacokinetic profiling in hamster revealed a stable concentration level (C$_{max}$ = 62 μM at 30 mg/kg single dose P.O., t$_{0.5}$ = 1.2 h) and reduced lung damage from acute SARS-CoV-2 infection in hamster recipients [87].
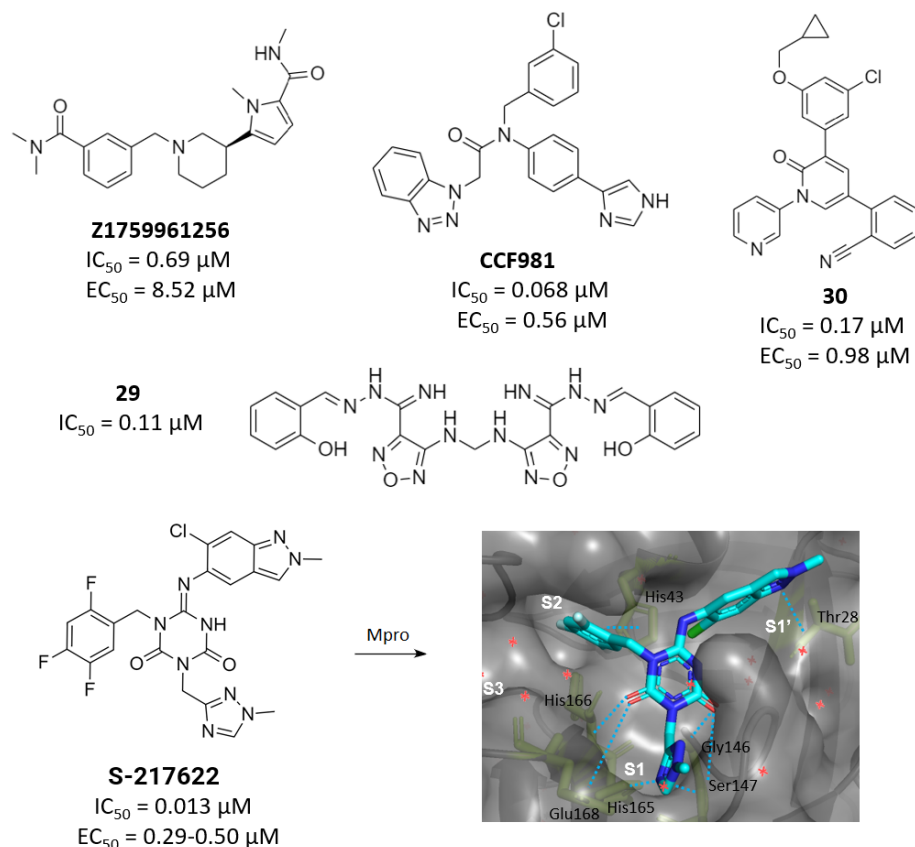

Figure 14. Chemical structures of noncompetitive M^{pro} inhibitors Z1759961256 [82], CCF981 [83], **29** [84], **30** [85], and S-217622 [86] with respective IC$_{50}$ and EC$_{50}$ values. The cloverleaf structure of S-217622 enables tight binding to M^{pro}'s active site (PDB 7vu6).

3. Allosteric Inhibitors

Aside from the Cys145-hosting main active site, several surface-exposed pockets of M^{pro} support catalytic activity assisting crucial enzyme dimerization or substrate processing. Experimentally, to date, six allosteric sites have been suggested, three of which are located at the dimerization interface and three more at distal surface regions (Figure 15). Since dimerization is integral for the activity of the main protease, allosteric inhibitors tar-

geting dimerization close sites seem especially valuable. While there are numerous studies reporting on in silico-generated noncompetitive inhibitors (and the interested reader is referred to those reviews for details, for example [88]), we focus solely on the few experimentally confirmed allosteric M^{pro} inhibitors that have been biologically validated and ideally crystallographically characterized. There are currently 35 PDB entries concerning noncompetitive inhibitors, possessing vastly different structural features and lipophilicity. The average size of cocrystallized allosteric inhibitors is about 200 Da less than that of covalently bound competitive inhibitors ($M_{w,aver} = 236 \pm 75$ g/mol).
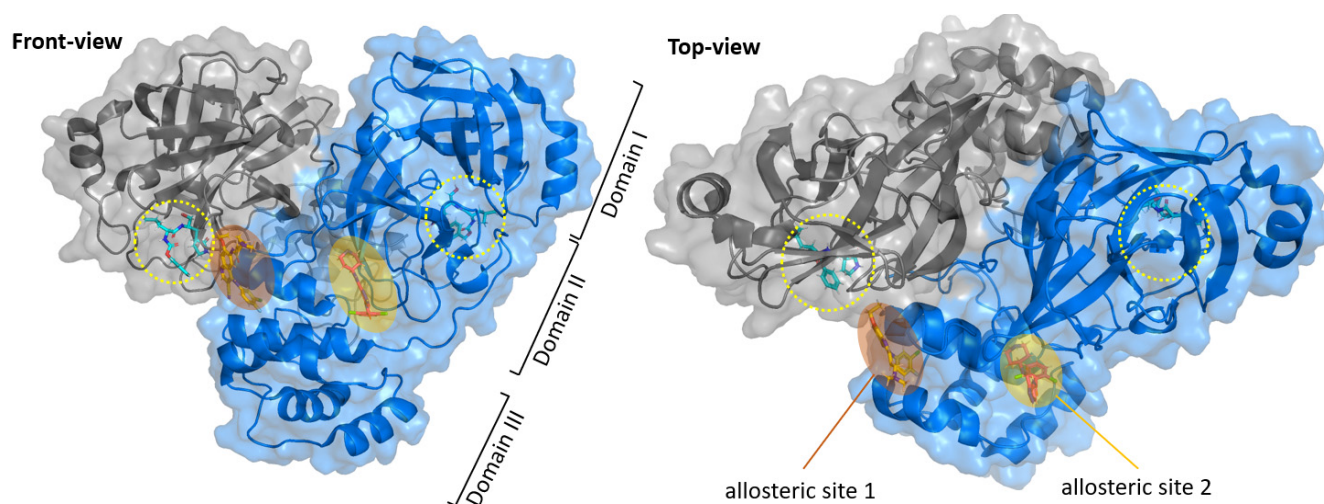

Figure 15. The dimeric structure of M^{pro} is vital for activity. Allosteric inhibitor binding sites are located near the dimerization site (allosteric site 1) or between domains (site 2) to impair conformational movement. The location of the active site in each monomer is indicated with a yellow circle.

A comprehensive drug screening effort of 5000 FDA- or near-FDA-approved drugs identified 37 M^{pro} inhibitors [89]. In cell-based assays, seven compounds had antiviral activity without toxicity. From their X-ray structures with M^{pro}, one drug showed noncovalent binding within the active site, while four more drugs were located at distal sites. The *S. aureus* antibacterial MUT056399 (Figure 16) coordinated near the active site and moderately inhibited SARS-CoV-2 viral activity ($EC_{50} = 38.2$ μM, $CC_{50} > 100$ μM; Table 3) in the Vero E6 cell assay. From the cocrystal structure, it is obvious that the diphenyl ether blocks access to the catalytic dyad, with other parts of the molecule binding to S1 and S2 pocket residues (PDB 7ap6). The flattened structure of the anticancer agent pelitinib covers a hydrophobic pocked within M^{pro}'s C-terminal dimerization domain, thereby interfering with activity-determining enzyme dimerization. It displays a potent antiviral effect ($EC_{50} = 1.25$ μM) and unfortunately, moderate VeroE6 cell toxicity ($CC_{50} = 14$ μM). While the 3-cyanoquinoline moiety interacts with the C-terminal helix around Ser301, the ethyl ether forms bridging interactions with a loop from the opposing protomer (PDB 7axm). Similarly, the vasodilator ifenprodil and the investigational chemokine RS-102895 (Figure 16) also bind to this allosteric site, resulting in moderate antiviral activity ($EC_{50} \geq 20$ μM) for both drugs (Table 3). Ifenprodil is undergoing clinical phase III studies to test its efficiency in acute intervention for hospitalized COVID-19 patients [90]. The same study identified a deep groove within the dimerization domain as a second allosteric site, which can be occupied by the investigational anticancer agent AT7519 (Figure 16) [89]. Binding to the grove is supported by van-der-Waals interactions of the chlorinated benzene ring with a hydrophobic residue wall as well as hydrogen-bonding with Gln110 and Arg298 (PDB 7aga). Mutational analysis demonstrated that Arg298 is crucial for dimerization, explaining AT7519's moderate antiviral effect ($EC_{50} = 25.2$ μM; $CC_{50} > 100$ μM). The anthelminthic drug niclosamide was identified as a wonder antiviral for various viruses, including SARS, MERS, ZIKV, HCV, and human adenovirus [91]. In a repurposing attempt,

Li and coworkers tested a library of 300 niclosamide derivatives for their anti-SARS-CoV-2 properties [92]. While several analogs were identified with low micromolar IC_{50} values and good antiviral effect but unfortunately also considerable cell toxicity, one compound, JMX0286 (Figure 16), stands out due to an increased selectivity index (IC_{50} = 4.8 µM, EC_{50} = 2.3 µM, CC_{50} = 53 µM, A549-hACE2 cells). Kinetic experiments showed a lowered maximum velocity but similar Km for inhibitor-treated samples, suggesting a noncompetitive inhibition mechanism. Molecular modeling points to a similar binding mode and allosteric site as that observed for AT7519. A recent clinical phase II trial showed no significant effect of niclosamide on decreasing the contagious period of SARS-CoV-2 infection [93]. Considering the structural similarity of M^{pro}'s binding site and its direct vicinity with that of thrombin (FactorXa), Chaves et al. were curious about the inhibitory effect of anticoagulants apixaban (Figure 16) and rivaroxaban [94]. In the in vitro assay, apixaban (IC_{50} = 0.01 µM) was superior to rivaroxaban (IC_{50} = 0.14 µM) and 21-fold more active than GC-376. Kinetic analysis suggests noncompetitive binding that seems to occur at the same allosteric site as that binding pelitinib (molecular docking). Apixaban inhibited SARS-CoV-2 replication in infected Calu-3 cells, with an EC_{50} of 1.84 µM, 60-times less potent than remdesivir, and showed in this assay a CC_{50} of 491 µM. Despite a low free plasma concentration (C_{max} = 0.55 mM) due to high binding affinity for albumin, apixabans free fraction was ~10-times higher than its SARS-CoV-2 M^{pro} affinity, serving as a good basis for further anti-coronaviral pharmacological studies. A structure-based virtual screening of 3.8 million small-molecule ligands recently identified three hits that showed promising complexation with the M^{pro} enzyme [95]. Among them, GR20 (Figure 16) showed with IC_{50} = 91.8 µM the best M^{pro} inhibition. Although competitive inhibition cannot be ruled out by the authors, kinetic analysis suggested a mixed inhibition model. Molecular docking gives the best fitting of GR20 into allosteric groove 2 (Figure 15), similar to that of the anticancer agent AT7519. From the natural pool of antivirals, the broad-spectrum drugs chebulagic acid and punicalagin have been demonstrated to show potent activity against M^{pro} [96]. Both drugs displayed IC_{50} and EC_{50} values in the lower micromolar range, with enzyme kinetic data indicating noncompetitive binding. From initial docking, it is suggested that these structurally extensive plant-based antivirals fit into a groove between domains II and III distal from the active site.

As an alternative anti-COVID-19 drug design, Xia and co-workers originally envisioned thiophilic metal complexation of the active site Cys145 using colloidal bismuth subcitrate (CBS) to inhibit M^{pro}'s activity [97]. Indeed, incubation of SARS-CoV-2 M^{pro} with CBS resulted in excellent inhibition (IC_{50} = 0.93 µM), but unexpectedly, k_{cat}/Km remained unchanged with both Km and v_{max} decreasing, indicating noncompetitive binding. Inductively coupled plasma mass spectrometry revealed an inhibitor:enzyme monomer ratio of 2. By mutational analysis, one binding site was identified as the C-terminal Cys300 residue, which is essential to stabilize the dimeric structure of M^{pro} [98]. The VeroE6 antiviral assay yielded a half maximal effective concentration of CBS against SARS-CoV-2 replication of 177.3 µM, sparking excitement for further drug optimization endeavors.

Based on the extended conformation of the native M^{pro} monomer, Geng and co-workers recently designed inhibitory nanobodies using the Nanoluc Binary Technology (nanoBiT) [99]. Application of a phage display library obtained 11 high-affinity nano-bodies from M^{pro}-immunized camel. An in vitro M^{pro} FRET assay indicated two antibodies as sub-micromolar M^{pro} binders (NB1A2 IC_{50} = 0.19 µM, NB2B4 IC_{50} = 0.12 µM; Table 3). Size-exclusion chromatography showed that binding to M^{pro} leads to dissociation to catalytically inactive monomers. Moreover, X-ray crystallographic analysis showed different epitopes for the two antibodies. In the cocrystal structure with NB2B4, the antibody is located at the α-helical domain of M^{pro}, distal from the catalytic site (PDB 7vfb). The other antibody binds instead to an epitope that overlaps with the substrate binding site, thus suggesting NB1A2 as not only an allosteric but also a competitive inhibitor (PDB 7vfa).
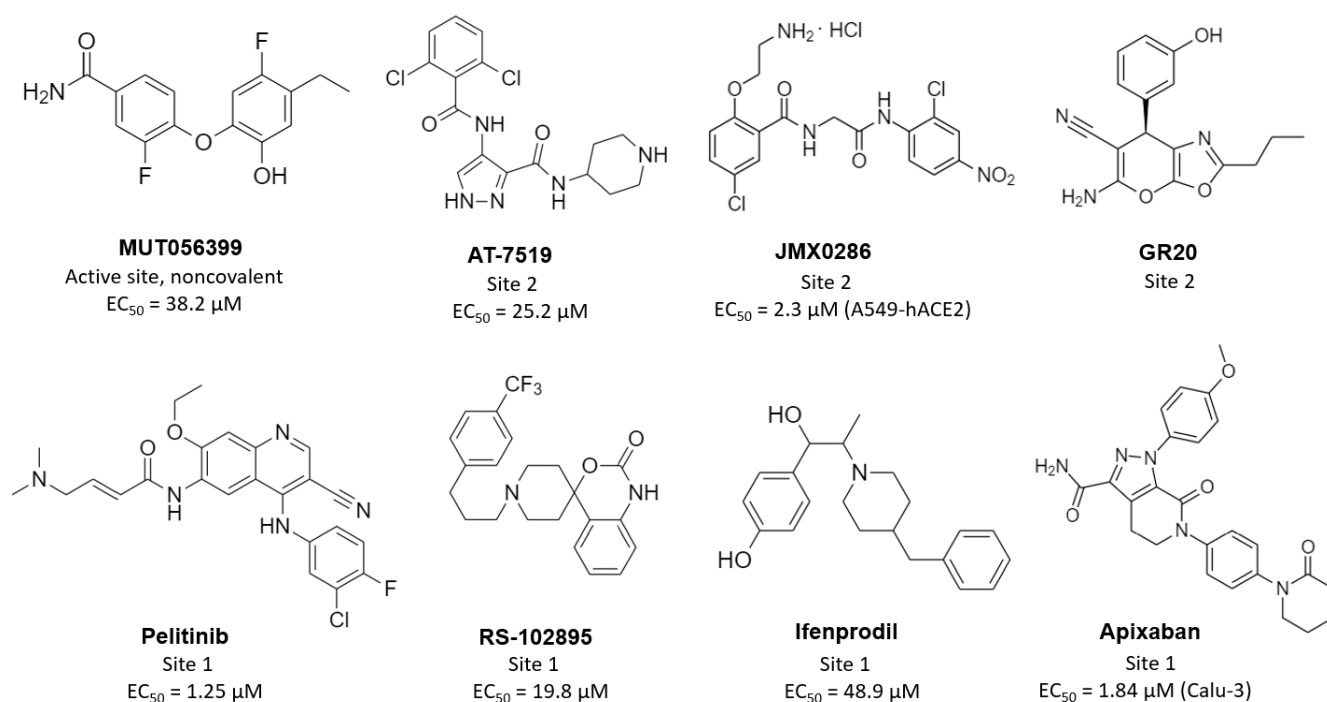
Figure 16. Structures of allosteric inhibitors MUT056399 [89], AT-7519 [89], pelitinib [89], RS-102895 [89], ifenprodil [89], JMX0286 [92], apixaban [94], and GR20 [95] with proposed binding sites and antiviral efficacy. Binding sites refer to Figure 15.

Table 3. In Vitro inhibition data of allosteric M^{pro} inhibitors and their PDB codes.

Inhibitor	Non-Competitive Binding in: [a]	IC$_{50}$ (μM)	EC$_{50}$ (μM) [b]	CC$_{50}$ (μM) [b]	PDB Code	Ref.
MUT056399	active site	-	38.2	>100	7ap6	[89]
pelitinib	allosteric site 1	-	1.25	14	7axm	[89]
ifenprodil	allosteric site 1	-	46.9	>100	7aqi	[89]
RS-102895	allosteric site 1	-	19.8	55	7abu	[89]
AT7519	allosteric site 2	-	25.2	>100	7aga	[89]
JMX0286	allosteric site 2 *	4.8	2.3 (A549-hACE2)	53(A549-hACE2)	-	[92]
apixaban	allosteric site 1 *	0.01	1.84 (Calu-3)	491(Calu-3)	-	[94]
GR20	allosteric site 2 *	91.8	-	-	-	[95]
chebulagic acid	alternative site	9.76	9.09	~100	-	[96]
punicalagin	alternative site	7.2	4.62	~100		[96]
colloidal bismuth-subcitrate (CBS)	alternative site	0.93	177.3	-	-	[97]
NB1A2	alternative site	0.19	-	-	7vfa	[99]
NB2B4	alternative site	0.12	-	-	7vfb	[99]

[a] An asterisk indicates predicted binding modes according to molecular docking. [b] Determined in VeroE6 cell assay unless stated otherwise.

4. Inhibitors in Action—Drug Performance in the Clinic

Several herein described SARS-CoV-2 antivirals that target its main protease, M^{pro}, have entered clinical studies and/or trials with varying success [100,101]. As mentioned before, reversible covalent inhibitors provide more beneficial pharmacokinetic data to qualify for clinical testing (Figure 17). Among the trial candidates, nirmatrelvir established the golden ticket to become the first covalent SARS-CoV-2 M^{pro} inhibitor, approved in combination with ritonavir for the treatment of mild-to-moderate COVID-19 in adults and pediatric patients 12 years or older. The US has committed to purchasing 20 million treatment courses, with close to 10 million treatment courses currently prescribed [102]. The

first meta-analysis studies indicate effectivity of the marketed drug paxlovid in reducing mortality and hospitalization rates in patients with COVID-19, with benefits especially for vulnerable cohorts including older patients, immunosuppressed patients, and patients with underlying neurological or cardiovascular disease [103,104]. Nonetheless, one must be aware of the limitations of a single target treatment regime, most importantly, the occurrence of viral resistance by mutational escape ("variants of concern"), as has been suggested in recent literature [105,106]. Recently, a higher reinfection rate after completing an antiviral treatment course compared to a control group has been observed in a prospective cohort study (preprint) [107]. Interestingly, this seems not to be attributable to virus mutation or impaired immunity but rather to a suboptimal drug exposure for certain patients [108], leaving room for further drug design and formulation development. Potential viral resistance has not only been recognized for paxlovid's M^{pro}-active ingredient nirmatrelvir but also for other late-stage M^{pro} antivirals such as GC376 and boceprevir. In fact, a study by Peng and co-workers investigated the development of resistance in a feline coronavirus (FIPV) under pressure from GC376 and found that a mutation in nsp12 of its main protease rendered the enzyme up to three times less susceptible for the inhibitor [109]. Encouraging data from cell culture studies hint that GC376 performs efficiently against M^{pro}'s from SARS-CoV-2 and various seasonal coronaviruses (NL63, 229E, and OC43), suggesting beneficial inhibition promiscuity of this drug that can be used as a basis for future structure development and antiviral testing [110]. This is in contrast to the molecular docking analysis that suggested comparable affinity of boceprevir and GC376 for the different analyzed coronaviral M^{pro} enzymes, leading the authors to caution against overinterpretation of in silico data during antiviral therapy development.
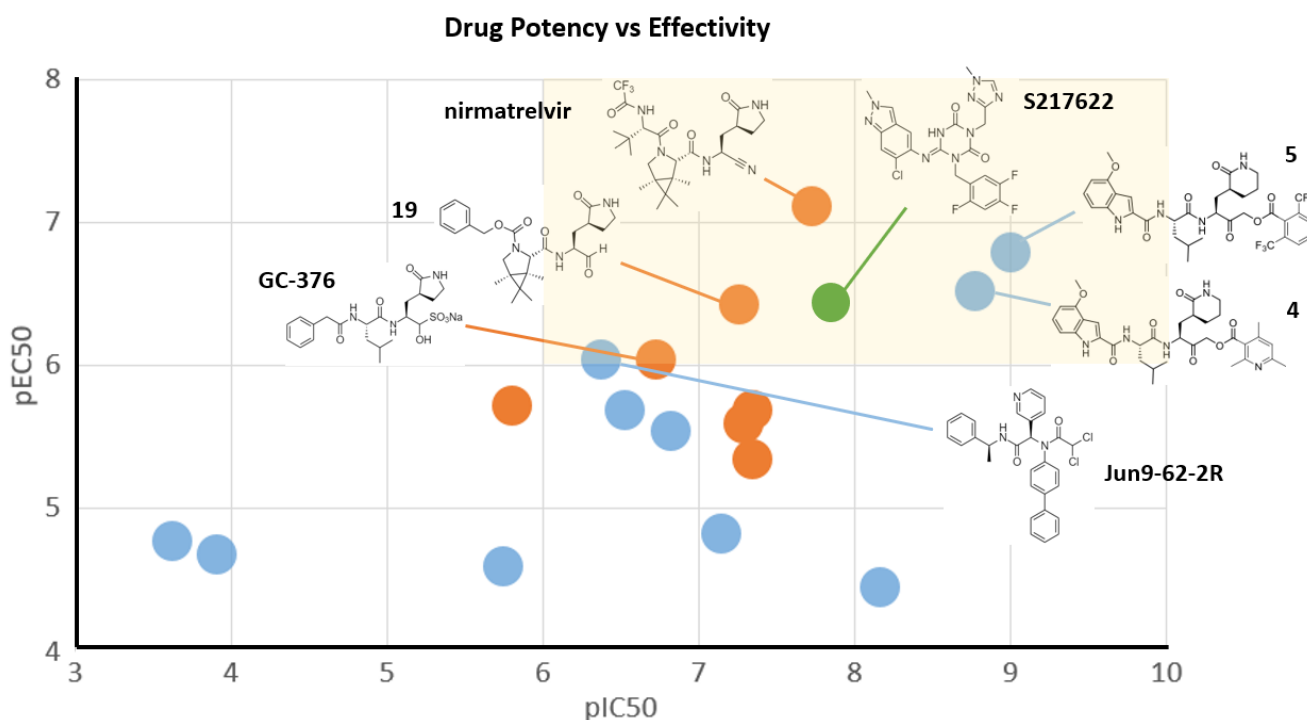

Figure 17. In Vitro performance of selected M^{pro} inhibitors. Compounds with nanomolar potency and efficacy are located in the yellow highlighted top corner of this graph, reflecting promising lead compounds or currently FDA-approved drugs (nirmatrelvir) to treat COVID-19. Irreversible, reversible, and noncovalent inhibitors are highlighted in blue, orange, and green, respectively.

5. Future Strategies/Outlook

The threat of a potentially uncontrollable pandemic has mobilized unprecedented scientific efforts to identify druggable targets of SARS-CoV-2. Influenced by successful past (corona)viral research, the main protease of the current coronavirus, M^{pro}, was identified

as one such target due to its critical role in virus replication and the expected low mutational susceptibility. Over the past three years, various research groups and companies around the globe entered the quest for potent SARS-CoV-2 M^{pro} antivirals, revealing at least two dozen lead structures with predominantly reversible warheads. About half a dozen peptidomimetic and small-molecule inhibitors have since entered clinical trials [101], with nirmatrelvir (Pfizer) receiving FDA emergency approval after successful pass of clinical trials and Shionogi's nonpeptidic S-217622 advancing to late-stage Phase III evaluation [86,111]. Central to the rapid discovery of vastly different inhibitor scaffolds was the accessibility of research data, catalyzed partly by extended open access policies of scientific journals and global molecular design initiatives such as COVID moonshot [112]. However, considering emerging reports of breakthrough infections after antiviral treatment and the constant threat of viral adaptability, and learning from the persistence of other viral epidemics such as HIV, the scientific community is challenged to be on the lookout for extended and alternative treatment options. One such strategy that has been proven effective, for example, in epidemiologic HIV management, is combination therapy, to explore synergistic drug effects and limit the potential mutational escape of mono-target antiviral therapies. Alternative viral targets with successfully developed inhibitors that can be co-targeted in a combination therapy include the RNA-dependent RNA polymerase (RdRP), the nucleocapsid protein (N), and the spike protein (S), among others [113]. An example of a synergistic combination therapy with high potential to further condemn viral replication is pairing the paxlovid drug nirmatrelvir with the RNA polymerase-attacking molnupiravir [114,115].

Another approach of enhanced antiviral combat considers alternative warhead chemistries to increase target specificity as well as drug bioavailability and clearance after successful therapy. An example that explores the chemical space around the reactive electrophilic warhead shows promising potential to finetune inhibitor properties to desired parameters solely by exchange of the reactive head group [116]. Aside from the already employed diversity of functional groups, novel chemistries that have the potential to improve target interaction can be derived from wider drug repurposing screens, including, for example, boronic acids, such as in ixazomib [117]. The example of colloidal bismuth subcitrate as a strong M^{pro} inhibitor highlights the potential of thiophilic metal complexes in anti-M^{pro} pharmacophore design [97]. Especially in the light of minimizing off-target effects, the excellent in vitro and in vivo performance of selected noncovalent leads such as S-217622 should be considered [86]. Lastly, available new drug delivery technologies can help to reduce dosage and unwanted side effects, potentially allowing the consideration of drug candidates with a smaller selectivity index that have previously been excluded [118]. Target overlap in vulnerable COVID-19 patients that are treated for pre-existing conditions, including cardiovascular and viral diseases, might lead to side-effects upon COVID-19 treatment. This can be desired if such interactions are synergistic, but drug exposure should be limited if contraindications have been identified. For such cases, new formulation technologies are anticipated to reduce the amount of active drug needed, minimizing off-target effects and avoiding drug accumulation. With these tools in development, new or improved SARS-CoV-2 M^{pro} inhibitors remain an exciting and beneficial avenue for the successful treatment and eradication of COVID-19 and its complications.

References

1. WHO Coronavirus (COVID-19) Dashboard | WHO Coronavirus (COVID-19) Dashboard with Vaccination Data. Available online: https://covid19.who.int/ (accessed on 12 December 2022).
2. Paul, D.; Pyne, N.; Paul, S. Mutation profile of SARS-CoV-2 spike protein and identification of potential multiple epitopes within spike protein for vaccine development against SARS-CoV-2. *Virusdisease* **2021**, *32*, 703–726. [CrossRef] [PubMed]
3. Tuekprakhon, A.; Nutalai, A.; Dijokaite-Guraliuc, A.; Zhou, D.; Ginn, H.M.; Selvaraj, M.; Liu, C.; Mentzer, A.J.; Supasa, P.; Duyvesteyn, H.M.E.; et al. Antibody escape of SARS-CoV-2 Omicron BA.4 and BA.5 from vaccine and BA.1 serum. *Cell* **2022**, *185*, 2422–2433. [CrossRef] [PubMed]
4. Khan, M.T.; Irfan, M.; Ahsan, H.; Ahmed, A.; Kaushik, A.C.; Khan, A.S.; Chinnasamy, S.; Ali, A.; Wei, D.-Q. Structures of SARS-CoV-2 RNA-Binding Proteins and Therapeutic Targets. *Intervirology* **2021**, *64*, 55–68. [CrossRef] [PubMed]
5. Amicone, M.; Borges, V.; Alves, M.J.; Isidro, J.; Zé-Zé, L.; Duarte, S.; Vieira, L.; Guiomar, R.; Gomes, J.P.; Gordo, I. Mutation rate of SARS-CoV-2 and emergence of mutators during experimental evolution. *Evol. Med. Public Health* **2022**, *10*, 142–155. [CrossRef]
6. Zhou, P.; Yang, X.L.; Wang, X.G.; Hu, B.; Zhang, L.; Zhang, W.; Si, H.R.; Zhu, Y.; Li, B.; Huang, C.L.; et al. A pneumonia outbreak associated with a new coronavirus of probable bat origin. *Nature* **2020**, *579*, 270–273. [CrossRef]
7. Zhang, L.; Lin, D.; Sun, X.; Curth, U.; Drosten, C.; Sauerhering, L.; Becker, S.; Rox, K.; Hilgenfeld, R. Crystal structure of SARS-CoV-2 main protease provides a basis for design of improved α-ketoamide inhibitors. *Science* **2020**, *368*, 409–412. [CrossRef] [PubMed]
8. Gao, X.; Qin, B.; Chen, P.; Zhu, K.; Hou, P.; Wojdyla, J.A.; Wang, M.; Cui, S. Crystal structure of SARS-CoV-2 papain-like protease. *Acta Pharm. Sin. B* **2021**, *11*, 237–245. [CrossRef]
9. Goyal, B.; Goyal, D. Targeting the Dimerization of the main protease of Coronaviruses: A potential broad-spectrum therapeutic strategy. *ACS Comb. Sci.* **2020**, *22*, 297–305. [CrossRef]
10. Tan, H.; Hu, Y.; Jadhav, P.; Tan, B.; Wang, J. Progress and challenges in targeting the SARS-CoV-2 papain-like protease. *J. Med. Chem.* **2022**, *65*, 7561–7580. [CrossRef]
11. Ferreira, J.C.; Fadl, S.; Villanueva, A.J.; Rabeh, W.M. Catalytic Dyad Residues His41 and Cys145 Impact the Catalytic Activity and Overall Conformational Fold of the Main SARS-CoV-2 Protease 3-Chymotrypsin-Like Protease. *Front. Chem.* **2021**, *9*, 692168. [CrossRef]
12. Gisdon, F.J.; Bombarda, E.; Ullmann, G.M. Serine and Cysteine Peptidases: So Similar, Yet Different. How the Active-Site Electrostatics Facilitates Different Reaction Mechanisms. *J. Phys. Chem. B* **2022**, *22*, 4035–4048. [CrossRef] [PubMed]
13. Nath, A.; Atkins, W.M. A Quantitative index of substrate promiscuity. *Biochemistry* **2008**, *47*, 157–166. [CrossRef] [PubMed]
14. Jin, Z.; Du, X.; Xu, Y.; Deng, Y.; Liu, M.; Zhao, Y.; Zhang, B.; Li, X.; Zhang, L.; Peng, C.; et al. Structure of M^{pro} from SARS-CoV-2 and discovery of its inhibitors. *Nature* **2020**, *582*, 289–293. [CrossRef] [PubMed]
15. Chen, L.; Gui, C.; Luo, X.; Yang, Q.; Günther, S.; Scandella, E.; Drosten, C.; Bai, D.; He, X.; Ludewig, B.; et al. Cinanserin is an inhibitor of the 3C-like proteinase of severe acute respiratory syndrome coronavirus and strongly reduces virus replication in vitro. *J. Virol.* **2005**, *79*, 7095–7103. [CrossRef]
16. Iketani, S.; Forouhar, F.; Liu, H.; Hong, S.J.; Lin, F.Y.; Nair, M.S.; Zask, A.; Huang, Y.; Xing, L.; Stockwell, B.R.; et al. Lead compounds for the development of SARS-CoV-2 3CL protease inhibitors. *Nat Commun.* **2021**, *12*, 2016. [CrossRef]
17. Amendola, G.; Ettari, R.; Previti, S.; Di Chio, C.; Messere, A.; Di Maro, S.; Hammerschmidt, S.J.; Zimmer, C.; Zimmermann, R.A.; Schirmeister, T.; et al. Lead discovery of SARSCoV-2 main protease inhibitors through covalent docking-based virtual screening. *J. Chem. Inf. Model.* **2021**, *61*, 2062–2073. [CrossRef]
18. Manandhar, A.; Srinivasulu, V.; Mohamad, H.; Tarazi, H.; Omar, H.; Colussi, D.J.; Gordon, J.; Childers, W.; Klein, M.L.; Al-Tel, T.H.; et al. Discovery of Novel Small-Molecule Inhibitors of SARS-CoV-2 Main Protease as Potential Leads for COVID-19 Treatment. *J. Chem. Inf. Model.* **2021**, *61*, 4745–4757. [CrossRef]
19. Zaidman, D.; Gehrtz, P.; Filep, M.; Fearon, D.; Gabizon, R.; Douangamath, A.; Prilusky, J.; Duberstein, S.; Cohen, G.; Owen, C.D.; et al. An automatic pipeline for the design of irreversible derivatives identifies a potent SARS-CoV-2 M^{pro} inhibitor. *Cell Chem. Biol.* **2021**, *28*, 1795–1806. [CrossRef]
20. Gossen, J.; Albani, S.; Hanke, A.; Joseph, B.P.; Bergh, C.; Kuzikov, M.; Costanzi, E.; Manelfi, C.; Storici, P.; Gribbon, P.; et al. A blueprint for high affinity SARS-CoV-2 M^{pro} inhibitors from activity-based compound library screening guided by analysis of protein dynamics. *ACS Pharmacol. Transl. Sci.* **2021**, *4*, 1079–1095. [CrossRef]
21. Chaves, O.A.; Fintelman-Rodrigues, N.; Wang, X.; Sacramento, C.Q.; Temerozo, J.R.; Ferreira, A.C.; Mattos, M.; Pereira-Dutra, F.; Bozza, P.T.; Castro-Faria-Neto, H.C.; et al. Commercially Available Flavonols Are Better SARS-CoV-2 Inhibitors than Isoflavone and Flavones. *Viruses* **2022**, *14*, 1458. [CrossRef]
22. Su, H.; Yao, S.; Zhao, W.; Zhang, Y.; Liu, J.; Shao, Q.; Wang, Q.; Li, M.; Xie, H.; Shang, W.; et al. Identification of pyrogallol as a warhead in design of covalent inhibitors for the SARS-CoV-2 3CL protease. *Nat. Commun.* **2021**, *12*, 3623. [CrossRef] [PubMed]
23. Xiao, T.; Cui, M.; Zheng, C.; Wang, M.; Sun, R.; Gao, D.; Bao, J.; Ren, S.; Yang, B.; Lin, J.; et al. Myricetin inhibits SARS-CoV-2 viral replication by targeting M^{pro} and ameliorates pulmonary inflammation. *Front. Pharmacol.* **2021**, *12*, 669642. [CrossRef]
24. Jin, Z.; Zhao, Y.; Sun, Y.; Zhang, B.; Wang, H.; Wu, Y.; Zhu, Y.; Zhu, C.; Hu, T.; Du, X.; et al. Structural basis for the inhibition of SARS-CoV-2 main protease by antineoplastic drug carmofur. *Nat. Struct. Mol. Biol.* **2020**, *27*, 529–532. [CrossRef] [PubMed]

25. Ma, C.; Hu, Y.; Townsend, J.A.; Lagarias, P.I.; Marty, M.T.; Kolocouris, A.; Wang, J. Ebselen, Disulfiram, Carmofur, PX-12, Tideglusib, and Shikonin Are Nonspecific Promiscuous SARS-CoV-2 Main Protease Inhibitors. *ACS Pharmacol. Transl. Sci.* **2020**, *3*, 1265–1277. [CrossRef] [PubMed]

26. Boras, B.; Jones, R.M.; Anson, B.J.; Arenson, D.; Aschenbrenner, L.; Bakowski, M.A.; Beutler, N.; Binder, J.; Chen, E.; Eng, H.; et al. Preclinical characterization of an intravenous coronavirus 3CL protease inhibitor for the potential treatment of COVID-19. *Nat. Commun.* **2021**, *12*, 6055. [CrossRef]

27. Bai, B.; Belovodskiy, A.; Hena, M.; Kandadai, A.S.; Joyce, M.A.; Saffran, H.A.; Shields, J.A.; Khan, M.B.; Arutyunova, E.; Lu, J.; et al. Peptidomimetic α-Acyloxymethylketone Warheads with Six-Membered Lactam P1 Glutamine Mimic: SARS-CoV-2 3CL Protease Inhibition, Coronavirus Antiviral Activity, and in vitro Biological Stability. *J. Med. Chem.* **2022**, *65*, 2905–2925. [CrossRef]

28. Hoffman, R.L.; Kania, R.S.; Brothers, M.A.; Davies, J.F.; Ferre, R.A.; Gajiwala, K.S.; He, M.; Hogan, R.J.; Kozminski, K.; Li, L.Y.; et al. Discovery of Ketone-Based Covalent Inhibitors of Coronavirus 3CL Proteases for the Potential Therapeutic Treatment of COVID-19. *J. Med. Chem.* **2020**, *63*, 12725–12747. [CrossRef]

29. Rasnick, D. Synthesis of peptide fluoromethyl ketones and the inhibition of human cathepsin B. *Anal. Biochem.* **1985**, *149*, 461–465. [CrossRef]

30. Eichhold, T.H.; Hookfin, E.B.; Taiwo, Y.O.; De, B.; Wehmeyer, K.R. Isolation and quantification of fluoroacetate in rat tissues, following dosing of Z-Phe-Ala-CH2-F, a peptidyl fluoromethyl ketone protease inhibitor. *J. Pharm. Biomed. Anal.* **1997**, *16*, 459–467. [CrossRef]

31. Stille, J.K.; Tjutrins, J.; Wang, G.; Venegas, F.A.; Hennecker, C.; Rueda, A.M.; Sharon, I.; Blaine, N.; Miron, C.E.; Pinus, S.; et al. Design, synthesis and in vitro evaluation of novel SARS-CoV-2 3CL^pro covalent inhibitors. *Eur. J. Med. Chem.* **2022**, *5*, 114046. [CrossRef]

32. Ma, C.; Xia, Z.; Sacco, M.D.; Hu, Y.; Townsend, J.A.; Meng, X.; Choza, J.; Tan, H.; Jang, J.; Gongora, M.V.; et al. Discovery of Di- and Trihaloacetamides as Covalent SARS-CoV-2 Main Protease Inhibitors with High Target Specificity. *J. Am. Chem. Soc.* **2021**, *143*, 20697–20709. [CrossRef] [PubMed]

33. Available online: https://cdn.dwi.gov.uk/wp-content/uploads/2020/10/27111054/DWI70_2_243.pdf (accessed on 12 December 2022).

34. Yamane, D.; Onitsuka, S.; Re, S.; Isogai, H.; Hamada, R.; Hiramoto, T.; Kawanishi, E.; Mizuguchi, K.; Shindo, N.; Ojida, A. Selective covalent targeting of SARS-CoV-2 main protease by enantiopure chlorofluoroacetamide. *Chem. Sci.* **2022**, *13*, 3027–3034. [CrossRef] [PubMed]

35. Moon, P.; Boike, L.; Dovala, D.; Henning, N.J.; Knapp, M.; Spradlin, J.N.; Ward, C.C.; Wolleb, H.; Zammit, C.M.; Fuller, D.; et al. Discovery of Potent Pyrazoline-Based Covalent SARS-CoV-2 Main Protease Inhibitors. *bioRxiv* **2022**. [CrossRef]

36. Xiong, M.; Nie, T.; Shao, Q.; Li, M.; Su, H.; Xu, Y. In silico screening-based discovery of novel covalent inhibitors of the SARS-CoV-2 3CL protease. *Eur. J. Med. Chem.* **2022**, *231*, 114130. [CrossRef]

37. Ettari, R.; Bonaccorso, C.; Micale, N.; Heindl, C.; Schirmeister, T.; Calabrò, M.L.; Grasso, S.; Zappalà, M. Development of Novel Peptidomimetics Containing a Vinyl Sulfone Moiety as Proteasome Inhibitors. *ChemMedChem* **2011**, *6*, 1228–1237. [CrossRef]

38. Ghosh, A.K.; Raghavaiah, J.; Shahabi, D.; Yadav, M.; Anson, B.J.; Lendy, E.K.; Hattori, S.; Higashi-Kuwata, N.; Mitsuya, H.; Mesecar, A.D. Indole Chloropyridinyl Ester-Derived SARS-CoV-2 3CL^pro Inhibitors: Enzyme Inhibition, Antiviral Efficacy, Structure–Activity Relationship, and X-ray Structural Studies. *J. Med. Chem.* **2021**, *64*, 14702–14714. [CrossRef]

39. Breidenbach, J.; Lemke, C.; Pillaiyar, T.; Schäkel, L.; Al Hamwi, G.; Diett, M.; Gedschold, R.; Geiger, N.; Lopez, V.; Mirza, S.; et al. Targeting the Main Protease of SARS-CoV-2: From the Establishment of High Throughput Screening to the Design of Tailored Inhibitors. *Angew. Chem. Int. Ed. Engl.* **2021**, *60*, 10423–10429. [CrossRef]

40. Ghosh, A.K.; Shahabi, D.; Yadav, M.; Kovela, S.; Anson, B.J.; Lendy, E.K.; Bonham, C.; Sirohi, D.; Brito-Sierra, C.A.; Hattori, S.I.; et al. Chloropyridinyl Esters of Nonsteroidal Anti-Inflammatory Agents and Related Derivatives as Potent SARS-CoV-2 3CL Protease Inhibitors. *Molecules* **2021**, *26*, 5782. [CrossRef]

41. Dai, W.; Zhang, B.; Jiang, X.M.; Su, H.; Li, J.; Zhao, Y.; Xie, X.; Jin, Z.; Peng, J.; Liu, F.; et al. Structure-based design of antiviral drug candidates targeting the SARS-CoV-2 main protease. *Science* **2020**, *368*, 1331–1335. [CrossRef]

42. Dai, W.; Jochmans, D.; Xie, H.; Yang, H.; Li, J.; Su, H.; Chang, D.; Wang, J.; Peng, J.; Zhu, L.; et al. Design, Synthesis, and Biological Evaluation of Peptidomimetic Aldehydes as Broad-Spectrum Inhibitors against Enterovirus and SARS-CoV-2. *J. Med. Chem.* **2022**, *65*, 2794–2808. [CrossRef]

43. Vuong, W.; Khan, M.B.; Fischer, C.; Arutyunova, E.; Lamer, T.; Shields, J.; Saffran, H.A.; McKay, R.T.; Van Belkum, M.J.; Joyce, M.A.; et al. Feline coronavirus drug inhibits the main protease of SARS-CoV-2 and blocks virus replication. *Nat. Commun.* **2020**, *11*, 4282. [CrossRef] [PubMed]

44. Fu, L.; Ye, F.; Feng, Y.; Yu, F.; Wang, Q.; Wu, Y.; Zhao, C.; Sun, H.; Huang, B.; Niu, P.; et al. Both Boceprevir and GC376 efficaciously inhibit SARS-CoV-2 by targeting its main protease. *Nat. Commun.* **2020**, *11*, 4417. [CrossRef] [PubMed]

45. Cáceres, C.J.; Cardenas-Garcia, S.; Carnaccini, S.; Seibert, B.; Rajao, D.S.; Wang, J.; Perez, D.R. Efficacy of GC-376 against SARS-CoV-2 virus infection in the K18 hACE2 transgenic mouse model. *Sci. Rep.* **2021**, *11*, 9609. [CrossRef] [PubMed]

46. Shi, Y.; Shuai, L.; Wen, Z.; Wang, C.; Yan, Y.; Jiao, Z.; Guo, F.; Fu, Z.F.; Chen, H.; Bu, Z.; et al. The preclinical inhibitor GS441524 in combination with GC376 efficaciously inhibited the proliferation of SARS-CoV-2 in the mouse respiratory tract. *Emerg. Microbes Infect.* **2021**, *10*, 481–492. [CrossRef]

47. Arutyunova, E.; Khan, M.B.; Fischer, C.; Lu, J.; Lamer, T.; Vuong, W.; van Belkum, M.J.; McKay, R.T.; Tyrrell, D.L.; Vederas, J.C.; et al. N-Terminal Finger Stabilizes the S1 Pocket for the Reversible Feline Drug GC376 in the SARS-CoV-2 M^{pro} Dimer. *J. Mol. Biol.* **2021**, *433*, 167003. [CrossRef]

48. Vuong, W.; Fischer, C.; Khan, M.B.; Van Belkum, M.J.; Lamer, T.; Willoughby, K.D.; Lu, J.; Arutyunova, E.; Joyce, M.A.; Saffran, H.A.; et al. Improved SARS-CoV-2 M^{pro} inhibitors based on feline antiviral drug GC376: Structural enhancements, increased solubility, and micellar studies. *Eur. J. Med. Chem.* **2021**, *222*, 113584. [CrossRef]

49. Sacco, M.D.; Ma, C.; Lagarias, P.; Gao, A.; Townsend, J.A.; Meng, X.; Dube, P.; Zhang, X.; Hu, Y.; Kitamura, N.; et al. Structure and inhibition of the SARS-CoV-2 main protease reveal strategy for developing dual inhibitors against M^{pro} and cathepsin L. *Sci. Adv.* **2020**, *6*, eabe0751. [CrossRef]

50. Liu, H.; Iketani, S.; Zask, A.; Khanizeman, N.; Bednarova, E.; Forouhar, F.; Fowler, B.; Hong, S.J.; Mohri, H.; Nair, M.S.; et al. Development of optimized drug-like small molecule inhibitors of the SARS-CoV-2 3CL protease for treatment of COVID-19. *Nat. Commun.* **2022**, *13*, 1891. [CrossRef]

51. Dampalla, C.S.; Kim, Y.; Bickmeier, N.; Rathnayake, A.D.; Nguyen, H.N.; Zheng, J.; Kashipathy, M.M.; Baird, M.A.; Battaile, K.P.; Lovell, S.; et al. Structure-Guided Design of Conformationally Constrained Cyclohexane Inhibitors of Severe Acute Respiratory Syndrome Coronavirus-2 3CL Protease. *J. Med. Chem.* **2021**, *64*, 10047–10058. [CrossRef]

52. Xia, Z.; Sacco, M.; Hu, Y.; Ma, C.; Meng, X.; Zhang, F.; Szeto, T.; Xiang, Y.; Chen, Y.; Wang, J. Rational Design of Hybrid SARS-CoV-2 Main Protease Inhibitors Guided by the Superimposed Cocrystal Structures with the Peptidomimetic Inhibitors GC-376, Telaprevir, and Boceprevir. *ACS Pharmacol. Transl. Sci.* **2021**, *4*, 1408–1421. [CrossRef]

53. Qiao, J.; Li, Y.S.; Zeng, R.; Liu, F.L.; Luo, R.H.; Huang, C.; Wang, Y.F.; Zhang, J.; Quan, B.; Shen, C.; et al. SARS-CoV-2 M^{pro} inhibitors with antiviral activity in a transgenic mouse model. *Science* **2021**, *371*, 1374–1378. [CrossRef] [PubMed]

54. Yang, K.S.; Ma, X.R.; Ma, Y.; Alugubelli, Y.R.; Scott, D.A.; Vatansever, E.C.; Drelich, A.K.; Sankaran, B.; Geng, Z.Z.; Blankenship, L.R.; et al. A Quick Route to Multiple Highly Potent SARS-CoV-2 Main Protease Inhibitors. *ChemMedChem* **2021**, *16*, 942–948. [CrossRef] [PubMed]

55. Ma, X.R.; Alugubelli, Y.R.; Ma, Y.; Vatansever, E.C.; Scott, D.A.; Qiao, Y.; Yu, G.; Xu, S.; Liu, W.R. MPI8 is Potent against SARS-CoV-2 by Inhibiting Dually and Selectively the SARS-CoV-2 Main Protease and the Host Cathepsin L. *ChemMedChem* **2022**, *17*, e202100456. [CrossRef] [PubMed]

56. Costanzi, E.; Kuzikov, M.; Esposito, F.; Albani, S.; Demitri, N.; Giabbai, B.; Camasta, M.; Tramontano, E.; Rossetti, G.; Zaliani, A.; et al. Structural and Biochemical Analysis of the Dual Inhibition of MG-132 against SARS-CoV-2 Main Protease (Mpro/3CLpro) and Human Cathepsin-L. *Int. J. Mol. Sci.* **2021**, *22*, 11779. [CrossRef]

57. Kuzikov, M.; Costanzi, E.; Reinshagen, J.; Esposito, F.; Vangeel, L.; Wolf, M.; Ellinger, B.; Claussen, C.; Geisslinger, G.; Corona, A.; et al. Identification of Inhibitors of SARS-CoV-2 3CL-Pro Enzymatic Activity Using a Small Molecule in vitro Repurposing Screen. *ACS Pharmacol. Transl. Sci.* **2021**, *4*, 1096–1110. [CrossRef] [PubMed]

58. Ma, C.; Sacco, M.D.; Hurst, B.; Townsend, J.A.; Hu, Y.; Szeto, T.; Zhang, X.; Tarbet, B.; Marty, M.T.; Chen, Y.; et al. Boceprevir, GC-376, and calpain inhibitors II, XII inhibit SARS-CoV-2 viral replication by targeting the viral main protease. *Cell Res.* **2020**, *30*, 678–692. [CrossRef]

59. Hu, Y.; Ma, C.; Szeto, T.; Hurst, B.; Tarbet, B.; Wang, J. Boceprevir, Calpain Inhibitors II and XII, and GC-376 Have Broad-Spectrum Antiviral Activity against Coronaviruses. *ACS Infect. Dis.* **2021**, *7*, 586–597. [CrossRef]

60. Zhang, L.; Lin, D.; Kusov, Y.; Nian, Y.; Ma, Q.; Wang, J.; Von Brunn, A.; Leyssen, P.; Lanko, K.; Neyts, J.; et al. α-Ketoamides as Broad-Spectrum Inhibitors of Coronavirus and Enterovirus Replication: Structure-Based Design, Synthesis, and Activity Assessment. *J. Med. Chem.* **2020**, *63*, 4562–4578. [CrossRef]

61. Oerlemans, R.; Ruiz-Moreno, A.J.; Cong, Y.; Dinesh Kumar, N.; Velasco-Velazquez, M.A.; Neochoritis, C.G.; Smith, J.; Reggiori, F.; Groves, M.R.; Dömling, A. Repurposing the HCV NS3-4A protease drug boceprevir as COVID-19 therapeutics. *RSC Med. Chem.* **2020**, *12*, 370–379. [CrossRef]

62. Kneller, D.W.; Phillips, G.; Weiss, K.L.; Zhang, Q.; Coates, L.; Kovalevsky, A. Direct Observation of Protonation State Modulation in SARS-CoV-2 Main Protease upon Inhibitor Binding with Neutron Crystallography. *J. Med. Chem.* **2021**, *64*, 4991–5000. [CrossRef]

63. Kneller, D.W.; Galanie, S.; Phillips, G.; O'Neill, H.M.; Coates, L.; Kovalevsky, A. Malleability of the SARS-CoV-2 3CL M^{pro} active-site cavity facilitates binding of clinical antivirals. *Structure* **2020**, *28*, 1313–1320. [CrossRef] [PubMed]

64. Mahmoud, A.; Mostafa, A.; Al-Karmalawy, A.A.; Zidan, A.; Abulkhair, H.S.; Mahmoud, S.H.; Shehata, M.; Elhefnawi, M.M.; Ali, M.A. Telaprevir is a potential drug for repurposing against SARS-CoV-2: Computational and in vitro studies. *Heliyon* **2021**, *7*, e07962. [CrossRef] [PubMed]

65. Wang, J.; Liang, B.; Chen, Y.; Fuk-Woo Chan, J.; Yuan, S.; Ye, H.; Nie, L.; Zhou, J.; Wu, Y.; Wu, M.; et al. A new class of α-ketoamide derivatives with potent anticancer and anti-SARS-CoV-2 activities. *Eur. J. Med. Chem.* **2021**, *215*, 113267. [CrossRef] [PubMed]

66. Chuck, C.; Chen, C.; Ke, Z.; Wan, D.C.; Chow, H.; Wong, K. Design, synthesis and crystallographic analysis of nitrile-based broad-spectrum peptidomimetic inhibitors for coronavirus 3C-like proteases. *Eur. J. Med. Chem.* **2013**, *59*, 1–6. [CrossRef]

67. Halford, B. The Path to Paxlovid. *ACS Cent. Sci.* **2022**, *8*, 405–407. [CrossRef]

68. Owen, D.R.; Allerton, C.M.N.; Anderson, A.S.; Aschenbrenner, L.; Avery, M.; Berritt, S.; Boras, B.; Cardin, R.D.; Carlo, A.; Coffman, K.J.; et al. An oral SARS-CoV-2 M^{pro} inhibitor clinical candidate for the treatment of COVID-19. *Science* **2021**, *374*, 1586–1593. [CrossRef]

69. Zhao, Y.; Fang, C.; Zhang, Q.; Zhang, R.; Zhao, X.; Duan, Y.; Wang, H.; Zhu, Y.; Feng, L.; Zhao, J.; et al. Crystal structure of SARS-CoV-2 main protease in complex with protease inhibitor PF-07321332. *Protein Cell* **2022**, *13*, 689–693. [CrossRef]

70. Abdelnabi, R.; Foo, C.S.; Jochmans, D.; Vangeel, L.; De Jonghe, S.; Augustijns, P.; Mols, R.; Weynand, B.; Wattanakul, T.; Hoglund, R.M.; et al. The oral protease inhibitor (PF-07321332) protects syrian hamsters against infection with SARS-CoV-2 variants of concern. *Nat. Commun.* **2022**, *13*, 719. [CrossRef]

71. Li, P.; Wang, Y.; Lavrijsen, M.; Lamers, M.M.; De Vries, A.C.; Rottier, R.J.; Bruno, M.J.; Peppelenbosch, M.P.; Haagmans, B.L.; Pan, Q. SARS-CoV-2 Omicron variant is highly sensitive to molnupiravir, nirmatrelvir, and the combination. *Cell Res.* **2022**, *32*, 322–324. [CrossRef]

72. Rai, D.K.; Yurgelonis, I.; McMonagle, P.; Rothan, H.A.; Hao, L.; Gribenko, A.; Titova, E.; Kreiswirth, B.; White, K.M.; Zhu, Y.; et al. Nirmatrelvir, an orally active M^pro inhibitor, is a potent inhibitor of SARS-CoV-2 variants of concern. *bioRxiv* **2022**. [CrossRef]

73. Greasley, S.E.; Noell, S.; Plotnikova, O.; Ferre, R.; Liu, W.; Bolanos, B.; Fennell, K.; Nicki, J.; Craig, T.; Zhu, Y.; et al. Structural basis for the in vitro efficacy of nirmatrelvir against SARS-CoV-2 variants. *J. Biol. Chem.* **2022**, *298*, 101972. [CrossRef] [PubMed]

74. Rosales, R.; McGovern, B.L.; Rodriguez, M.L.; Rai, D.K.; Cardin, R.D.; Anderson, A.S.; PSP Study Group; Sordillo, E.M.; van Bakel, H.; Simon, V.; et al. Nirmatrelvir, molnupiravir, and remdesivir maintain potent in vitro activity against the SARS-CoV-2 Omicron variant. *bioRxiv* **2022**. [CrossRef]

75. Singh, R.S.P.; Toussi, S.S.; Hackman, F.; Chan, P.L.; Rao, R.; Allen, R.; Van Eyck, L.; Pawlak, S.; Kadar, E.P.; Clark, F.; et al. Innovative Randomized Phase I Study and Dosing Regimen Selection to Accelerate and Inform Pivotal COVID-19 Trial of Nirmatrelvir. *Clin. Pharmacol. Ther.* **2022**, *112*, 101–111. [CrossRef] [PubMed]

76. Toussi, S.S.; Neutel, J.M.; Navarro, J.; Preston, R.A.; Shi, H.; Kavetska, O.; LaBadie, R.R.; Binks, M.; Chan, P.L.S.; Demers, N.; et al. Pharmacokinetics of Oral Nirmatrelvir/Ritonavir, a Protease Inhibitor for Treatment of COVID-19, in Subjects with Renal Impairment. *Clin. Pharmacol. Ther.* **2022**, *112*, 892–900. [CrossRef]

77. Owen, D.R.; Pettersson, M.Y.; Reese, M.R.; Sammons, M.F.; Tuttle, J.B.; Verhoest, P.R.; Wei, L.; Yang, Q.; Yang, X. Nitrile-Containing Antiviral Compounds, World Intellectual Property Organization International. Bureau Patent WO 2021/250648A1, 16 December 2021.

78. Bai, B.; Arutyunova, E.; Khan, M.B.; Lu, J.; Joyce, M.A.; Saffran, H.A.; Shields, J.A.; Kandadai, A.S.; Belovodskiy, A.; Hena, M.; et al. Peptidomimetic nitrile warheads as SARS-CoV-2 3CL protease inhibitors. *RSC Med. Chem.* **2021**, *12*, 1722–1730. [CrossRef] [PubMed]

79. Amporndanai, K.; Meng, X.; Shang, W.; Jin, Z.; Rogers, M.; Zhao, Y.; Rao, Z.; Liu, Z.J.; Yang, H.; Zhang, L.; et al. Inhibition mechanism of SARS-CoV-2 main protease by ebselen and its derivatives. *Nat. Commun.* **2021**, *12*, 3061. [CrossRef]

80. Madabeni, A.; Nogara, P.A.; Omage, F.B.; Rocha, J.B.T.; Orian, L. Mechanistic insight into SARS-CoV-2 M^pro inhibition by organoselenides: The ebselen case study. *Appl. Sci.* **2021**, *11*, 6291. [CrossRef]

81. Parise, A.; Romeo, I.; Russo, N.; Marino, T. The Se-S bond formation in the covalent inhibition mechanism of SARS-CoV-2 main protease by ebselen-like inhibitors: A computational study. *Int. J. Mol. Sci.* **2021**, *22*, 9792. [CrossRef]

82. Yang, J.; Lin, X.; Xing, N.; Zhang, Z.; Zhang, H.; Wu, H.; Xue, W. Structure-Based Discovery of Novel Nonpeptide Inhibitors Targeting SARS-CoV-2 Mpro. *J. Chem. Inf. Model.* **2021**, *61*, 3917–3926. [CrossRef]

83. Han, S.H.; Goins, C.M.; Arya, T.; Shin, W.J.; Maw, J.; Hooper, A.; Sonawane, D.P.; Porter, M.R.; Bannister, B.E.; Crouch, R.D.; et al. Structure-Based Optimization of ML300-Derived, Noncovalent Inhibitors Targeting the Severe Acute Respiratory Syndrome Coronavirus 3CL Protease (SARS-CoV-2 3CL^pro). *J. Med. Chem.* **2022**, *65*, 2880–2904. [CrossRef]

84. Elseginy, S.A.; Fayed, B.; Hamdy, R.; Mahrous, N.; Mostafa, A.; Almehdi, A.M.; Soliman, S.S.M. Promising anti-SARS-CoV-2 drugs by effective dual targeting against the viral and host proteases. *Bioorg. Med. Chem. Lett.* **2021**, *43*, 128099. [CrossRef] [PubMed]

85. Zhang, C.H.; Stone, E.A.; Deshmukh, M.; Ippolito, J.A.; Ghahremanpour, M.M.; Tirado-Rives, J.; Spasov, K.A.; Zhang, S.; Takeo, Y.; Kudalkar, S.N.; et al. Potent Noncovalent Inhibitors of the Main Protease of SARS-CoV-2 from Molecular Sculpting of the Drug Perampanel Guided by Free Energy Perturbation Calculations. *ACS Cent. Sci.* **2021**, *7*, 467–475. [CrossRef] [PubMed]

86. Unoh, Y.; Uehara, S.; Nakahara, K.; Nobori, H.; Yamatsu, Y.; Yamamoto, S.; Maruyama, Y.; Taoda, Y.; Kasamatsu, K.; Suto, T.; et al. Discovery of S-217622, a Noncovalent Oral SARS-CoV-2 3CL Protease Inhibitor Clinical Candidate for Treating COVID-19. *J. Med. Chem.* **2022**, *65*, 6499–6512. [CrossRef] [PubMed]

87. Sasaki, M.; Tabata, K.; Kishimoto, M.; Itakura, Y.; Kobayashi, H.; Ariizumi, T.; Uemura, K.; Toba, S.; Kusakabe, S.; Maruyama, Y.; et al. S-217622, a SARS-CoV-2 main protease inhibitor, decreases viral load and ameliorates COVID-19 severity in hamsters. *Sci. Transl. Med.* **2022**, *15*, eabq4064. [CrossRef]

88. Alzyoud, L.; Ghattas, M.A.; Atatreh, N. Allosteric Binding Sites of the SARS-CoV-2 Main Protease: Potential Targets for Broad-Spectrum Anti-Coronavirus Agents. *Drug Des. Devel. Ther.* **2022**, *16*, 2463–2478. [CrossRef]

89. Günther, S.; Reinke, P.Y.A.; Fernández-García, Y.; Lieske, J.; Lane, T.J.; Ginn, H.M.; Koua, F.H.M.; Ehrt, C.; Ewert, W.; Oberthuer, D.; et al. X-ray screening identifies active site and allosteric inhibitors of SARS-CoV-2 main protease. *Science* **2021**, *372*, 642–646. [CrossRef]

90. Safety and Efficacy of NP-120 (Ifenprodil) for the Treatment of Hospitalized Patient with Confirmed COVID-19 Disease. Available online: https://beta.clinicaltrials.gov/study/NCT04382924?tab=results (accessed on 12 December 2022).

91. Xu, J.; Shi, P.Y.; Li, H.; Zhou, J. Broad Spectrum Antiviral Agent Niclosamide and Its Therapeutic Potential. *ACS Infect. Dis.* **2020**, *6*, 909–915. [CrossRef]

92. Samrat, S.K.; Xu, J.; Xie, X.; Gianti, E.; Chen, H.; Zou, J.; Pattis, J.G.; Elokely, K.; Lee, H.; Li, Z.; et al. Allosteric inhibitors of the main protease of SARS-CoV-2. *Antiviral Res.* **2022**, *205*, 105381. [CrossRef]

93. Cairns, D.M.; Dulko, D.; Griffiths, J.K.; Golan, Y.; Cohen, T.; Trinquart, L.; Price, L.L.; Beaulac, K.R.; Selker, H.P. Efficacy of Niclosamide vs Placebo in SARS-CoV-2 Respiratory Viral Clearance, Viral Shedding, and Duration of Symptoms Among Patients with Mild to Moderate COVID-19: A Phase 2 Randomized Clinical Trial. *JAMA Netw. Open.* **2022**, *5*, e2144942. [CrossRef]

94. Chaves, O.A.; Sacramento, C.Q.; Fintelman-Rodrigues, N.; Temerozo, J.R.; Pereira-Dutra, F.; Mizurini, D.M.; Monteiro, R.Q.; Vazquez, L.; Bozza, P.T.; Castro-Faria-Neto, H.C.; et al. Apixaban, an orally available anticoagulant, inhibits SARS-CoV-2 replication and its major protease in a non-competitive way. *J. Mol. Cell Biol.* **2022**, *14*, mjac039. [CrossRef]

95. Mahgoub, R.E.; Mohamed, F.E.; Alzyoud, L.; Ali, B.R.; Ferreira, J.; Rabeh, W.M.; AlNeyadi, S.S.; Atatreh, N.; Ghattas, M.A. The Discovery of Small Allosteric and Active Site Inhibitors of the SARS-CoV-2 Main Protease via Structure-Based Virtual Screening and Biological Evaluation. *Molecules* **2022**, *27*, 6710. [CrossRef]

96. Du, R.; Cooper, L.; Chen, Z.; Lee, H.; Rong, L.; Cui, Q. Discovery of chebulagic acid and punicalagin as novel allosteric inhibitors of SARS-CoV-2 3CL^{pro}. *Antiviral Res.* **2021**, *190*, 105075. [CrossRef] [PubMed]

97. Tao, X.; Zhang, L.; Du, L.; Liao, R.; Cai, H.; Lu, K.; Zhao, Z.; Xie, Y.; Wang, P.H.; Pan, J.A.; et al. Allosteric inhibition of SARS-CoV-2 3CL protease by colloidal bismuth subcitrate. *Chem. Sci.* **2021**, *12*, 14098–14102. [CrossRef] [PubMed]

98. El-Baba, T.J.; Lutomski, C.A.; Kantsadi, A.L.; Malla, T.R.; John, T.; Mikhailov, V.; Bolla, J.R.; Schofield, C.J.; Zitzmann, N.; Vakonakis, I.; et al. Allosteric Inhibition of the SARS-CoV-2 Main Protease: Insights from Mass Spectrometry Based Assays. *Angew. Chem. Int. Ed.* **2020**, *59*, 23544–23548. [CrossRef] [PubMed]

99. Sun, Z.; Wang, L.; Li, X.; Fan, C.; Xu, J.; Shi, Z.; Qiao, H.; Lan, Z.; Zhang, X.; Li, L.; et al. An extended conformation of SARS-CoV-2 main protease reveals allosteric targets. *Proc. Natl. Acad. Sci. USA* **2022**, *119*, e2120913119. [CrossRef]

100. Brüssow, H. Clinical trials with antiviral drugs against COVID-19: Some progress and many shattered hopes. *Environ. Microbiol.* **2021**, *23*, 6364–6376. [CrossRef]

101. Cully, M. A tale of two antiviral targets—And the COVID-19 drugs that bind them. *Nat. Rev. Drug Discov.* **2022**, *21*, 3–5. [CrossRef]

102. COVID-19 Therapeutics Thresholds, Orders, and Replenishment by Jurisdiction. Available online: https://aspr.hhs.gov/COVID-19/Therapeutics/Orders/Pages/default.aspx (accessed on 12 December 2022).

103. Wen, W.; Chen, C.; Tang, J.; Wang, C.; Zhou, M.; Cheng, Y.; Zhou, X.; Wu, Q.; Zhang, X.; Feng, Z.; et al. Efficacy and safety of three new oral antiviral treatment (molnupiravir, fluvoxamine and Paxlovid) for COVID-19: A meta-analysis. *Ann. Med.* **2022**, *54*, 516–523. [CrossRef]

104. Najjar-Debbiny, R.; Gronich, N.; Weber, G.; Khoury, J.; Amar, M.; Stein, N.; Goldstein, L.H.; Saliba, W. Effectiveness of Paxlovid in Reducing Severe COVID-19 and Mortality in High-Risk Patients. *Clin. Infect. Dis.* **2022**, ciac443. [CrossRef]

105. Heilmann, E.; Costacurta, F.; Moghadasi, S.A.; Ye, C.; Pavan, M.; Bassani, D.; Volland, A.; Ascher, C.; Weiss, A.K.H.; Bante, D.; et al. SARS-CoV-2 3CL^{pro} mutations selected in a VSV-based system confer resistance to nirmatrelvir, ensitrelvir, and GC376. *Sci. Transl. Med.* **2022**, eabq7360. [CrossRef]

106. Lowe, D. Paxlovid Resistance: Is It Just a Matter of Time Now? | Science | AAAS. Available online: https://www.science.org/content/blog-post/paxlovid-resistance-it-just-matter-time-now (accessed on 12 December 2022).

107. Pandit, J.A.; Radin, J.M.; Chiang, D.; Spencer, E.; Pawelek, J.; Diwan, M.; Roumani, L.; Mina, M. The paxlovid rebound study: A prospective cohort study to evaluate viral and symptom rebound differences between Paxlovid and untreated COVID-19 participants. *medRxiv* **2022**. [CrossRef]

108. Carlin, A.F.; Clark, A.E.; Chaillon, A.; Garretson, A.F.; Bray, W.; Porrachia, M.; Santos, A.L.T.; Rana, T.M.; Smith, D.M. Virologic and immunologic characterization of coronavirus diseases 2019 recrudescence after nirmatrelvir/ritonavir treatment. *Clin. Infect. Dis.* **2022**, ciac496. [CrossRef] [PubMed]

109. Jiao, Z.; Yan, Y.; Chen, Y.; Wang, G.; Wang, X.; Li, L.; Yang, M.; Hu, X.; Guo, Y.; Shi, Y.; et al. Adaptive Mutation in the Main Protease Cleavage Site of Feline Coronavirus Renders the Virus More Resistant to Main Protease Inhibitors. *J. Virol.* **2022**, *96*, e0090722. [CrossRef] [PubMed]

110. Wang, Y.; Li, P.; Lavrijsen, M.; Li, Y.; Ma, Z.; Peppelenbosch, M.P.; Baig, M.S.; Pan, Q. Differing pan-coronavirus antiviral potency of boceprevir and GC376 in vitro despite discordant molecular docking predictions. *Arch. Virol.* **2022**, *167*, 1125–1130. [CrossRef] [PubMed]

111. A Study to Compare S-217622 with Placebo in Non-Hospitalized Participants with COVID-19 (SCORPIO-HR). Available online: https://clinicaltrials.gov/ct2/show/NCT05305547 (accessed on 12 December 2022).

112. The COVID Moonshot Consortium; Achdout, H.; Aimon, A.; Bar-David, E.; Barr, H.; Ben-Shmuel, A.; Bennett, J.; Bobby, M.L.; Borden, B.; Bowman, G.R.; et al. Open science discovery of oral non-covalent SARS-CoV-2 main protease inhibitor therapeutics. *bioRxiv* **2020**. [CrossRef]

113. Kulkarni, S.A.; Ingale, K. In silico approaches for drug repurposing for SARS-CoV-2 infection. In *The Coronavirus Pandemic and the Future: Virology, Epidemiology, Translational Toxicology and Therapeutics*, 1st ed.; Waters, M.D., Dhawan, A., Marrs, T., Anderson, D., Warren, S., Hughes, C.L., Eds.; RSC Publishing: Croydon, UK, 2022; Volume 2, pp. 1–80.

114. Gidari, A.; Sabbatini, S.; Schiaroli, E.; Bastianelli, S.; Pierucci, S.; Busti, C.; Comez, L.; Libera, V.; Macchiarulo, A.; Paciaroni, A.; et al. The Combination of Molnupiravir with Nirmatrelvir or GC376 Has a Synergic Role in the Inhibition of SARS-CoV-2 Replication In Vitro. *Microorganisms* **2022**, *10*, 1475. [CrossRef] [PubMed]

115. Wagoner, J.; Herring, S.; Hsiang, T.Y.; Ianevski, A.; Biering, S.B.; Xu, S.; Hoffmann, M.; Pöhlmann, S.; Gale, M., Jr.; Aittokallio, T.; et al. Combinations of Host- and Virus-Targeting Antiviral Drugs Confer Synergistic Suppression of SARS-CoV-2. *Microbiol. Spectr.* **2022**, *10*, e0333122. [CrossRef]
116. Vankadara, S.; Dawson, M.D.; Fong, J.Y.; Oh, Q.Y.; Ang, Q.A.; Liu, B.; Chang, H.Y.; Koh, J.; Koh, X.; Tan, Q.W.; et al. A Warhead Substitution Study on the Coronavirus Main Protease Inhibitor Nirmatrelvir. ACS Med. *Chem. Lett.* **2022**, *13*, 1345–1350.
117. Vázquez-Mendoza, L.H.; Mendoza-Figueroa, H.L.; García-Vázquez, J.B.; Correa-Basurto, J.; García-Machorro, J. In Silico Drug Repositioning to Target the SARS-CoV-2 Main Protease as Covalent Inhibitors Employing a Combined Structure-Based Virtual Screening Strategy of Pharmacophore Models and Covalent Docking. *Int. J. Mol. Sci.* **2022**, *23*, 3987. [CrossRef]
118. Williams, R. Improved Formulations to Enable Stable Delivery of Biologics. *BioPharm. Int.* **2022**, *35*, 46–49.